X-RAY DIFFRACTION STUDIES ON LITHIUM INTERCALATED MoS_2

by

DAVID STANLEY WAINWRIGHT

B.Sc. (Honours), Dalhousie University, 1976

A THESIS SUBMITTED IN PARTIAL FULFILLMENT OF

THE REQUIREMENTS FOR THE DEGREE OF

MASTER OF SCIENCE

in

THE FACULTY OF GRADUATE STUDIES

the Department of

Physics

We accept this thesis as conforming

to the required standard

THE UNIVERSITY OF BRITISH COLUMBIA

November, 1978

In presenting this thesis in partial fulfilment of the requirements for an advanced degree at the University of British Columbia, I agree that the Library shall make it freely available for reference and study. I further agree that permission for extensive copying of this thesis for scholarly purposes may be granted by the Head of my Department or by his representatives. It is understood that copying or publication of this thesis for financial gain shall not be allowed without my written permission.

Department of Physics

The University of British Columbia
2075 Wesbrook Place
Vancouver, Canada
V6T 1W5

Date Oct. 31, 1978

ABSTRACT

Li_xMoS_2 samples were prepared by cathodically intercalating a MoS_2 powder cathode with lithium. X-ray diffraction patterns of these samples were taken using the Debye-Scherrer method. From these patterns, the crystal structure of the lithium intercalated MoS_2 was determined as a function of cell voltage.

There is no apparent change in the powder patterns until a phase transition occurs in the sample at ≃ 1.1 V. This transition appears to involve a slipping of lattice planes in the MoS_2 crystal. Straining of the lattice is evident after this phase transition takes place. Non-uniform straining blurred the X-ray pictures with the result that the structure of the new phase could not be unambiguously determined. It does seem certain though, that an aligning of the Mo atoms takes place in this transition.

The new phase could be fit to a hexagonal unit cell. The lattice parameters were measured over a charge-discharge cycle in the new phase. The unit cell parameters reversibly change throughout a cycle, implying that intercalation takes place. The c axis exhibits a maximum with increasing lithium content, while the a axis increases monotonically. The volume of the unit cell increases smoothly however, reaching a maximum value some 15% larger than the original.

Another phase transition may take place at ≃ 0.55 V. Samples discharged below this voltage appear almost amorphous in the powder patterns, possibly due to extreme non-uniform straining of the lattice.

Some decomposition products of the Li-MoS_2 cells have also been discovered.

TABLE OF CONTENTS

LIST OF FIGURES

LIST OF TABLES

ACKNOWLEDGEMENTS

Many thanks go to my supervisor Rudi Haering who somehow always found the time to give me help on this project.

A group at U.B.C. has been studying the Li-MoS_2 battery since 1977, and much of this thesis is based upon work done by members of this group. I would then also wish to thank

Dr. Jim Stiles
Dr. Klaus Brandt
Nelson Shen
Ross McKinnon
Ulrich Sacken
Chris Hodgson
and Brendon Wong

for contributions they have made.

Peter Haas prepared the figures presented in this thesis, and his work is much appreciated.

I am grateful to the National Research Council for their financial support in the form of a scholarship.

1. Introduction

The desire to create a high energy density battery for use in electric vehicles has aroused interest in the group of transition metal dichalcogenides, many of which form layer structures. At the present time, several layer compounds are being tested as candidates for cell cathodes. Scientists at Exxon are working with TiS_2, while researchers at Bell Labs are studying VS_2. (Results of these studies can be found in papers by M.S. Whittingham 1976 and D.W. Murphy, J.N. Carides, et al 1977 respectively.) Our group is working with the mineral molybdenite, MoS_2, the only transition metal dichalcogenide which occurs naturally in significant quantities.

In many layer compounds, it is possible to insert, or intercalate, specific substances between the layers of the material. The process of intercalation is not a newly discovered phenomenon, having been investigated in graphite as early as 1841 (C. Schafhäutl). The fact that, in the aforementioned compounds, the intercalated material can be removed without destroying the host lattice makes these materials look like good candidates for secondary (rechargeable) battery cathodes.

The state of discharge of our batteries depends on the extent to which the MoS_2 is intercalated. The purpose of this thesis was to determine, by X-ray diffraction techniques, the crystal structure of the MoS_2 cathode as a function of the state of discharge.

1.1 Layer compounds

The layered transition metal dichalcogenides have the general form shown in Fig. 1. The transition metal atoms, M, are sandwiched between the

(a) General form

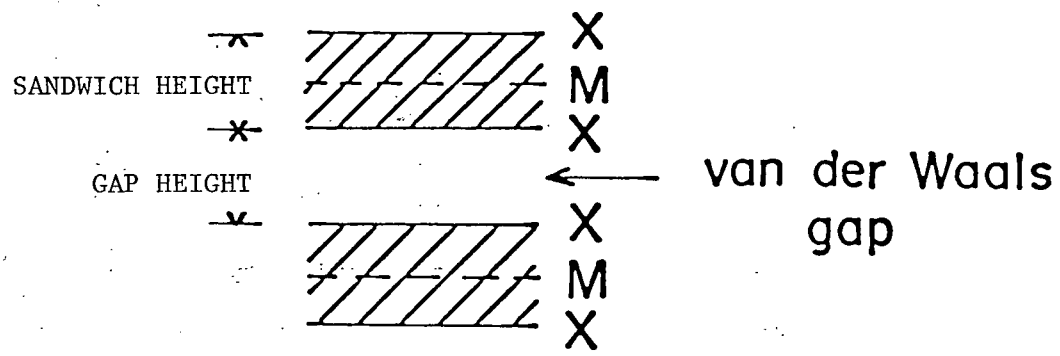

(b) Coordination units for MX_2 layer structures

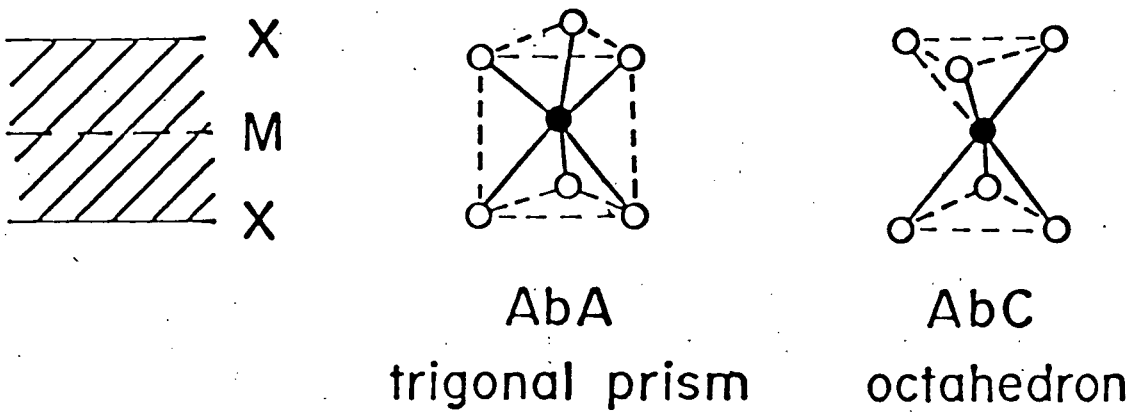

Fig. 1 - Layered transition metal dichalcogenides

(after Wilson and Yoffe 1969)

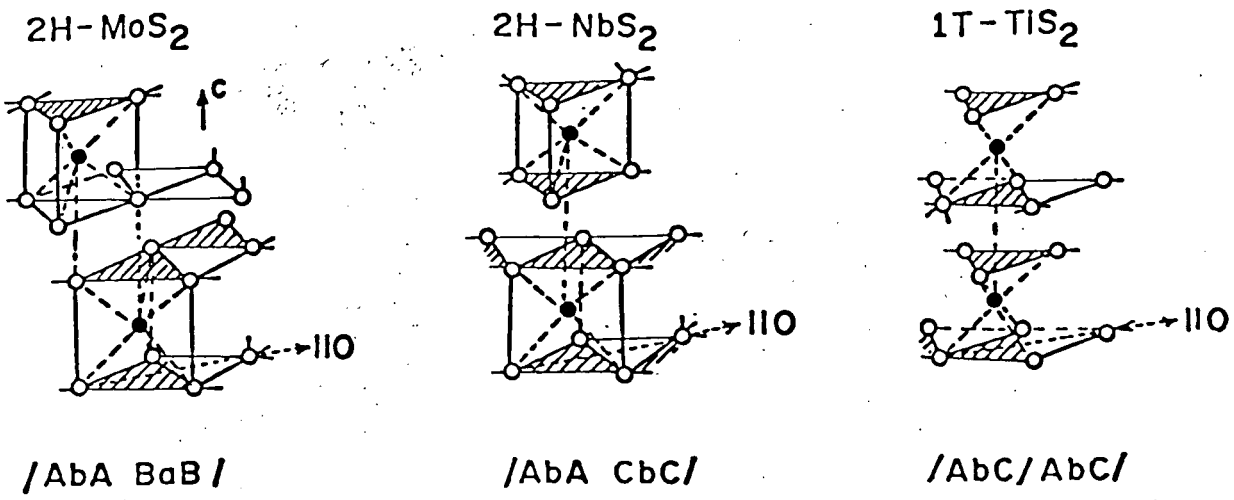

(a)

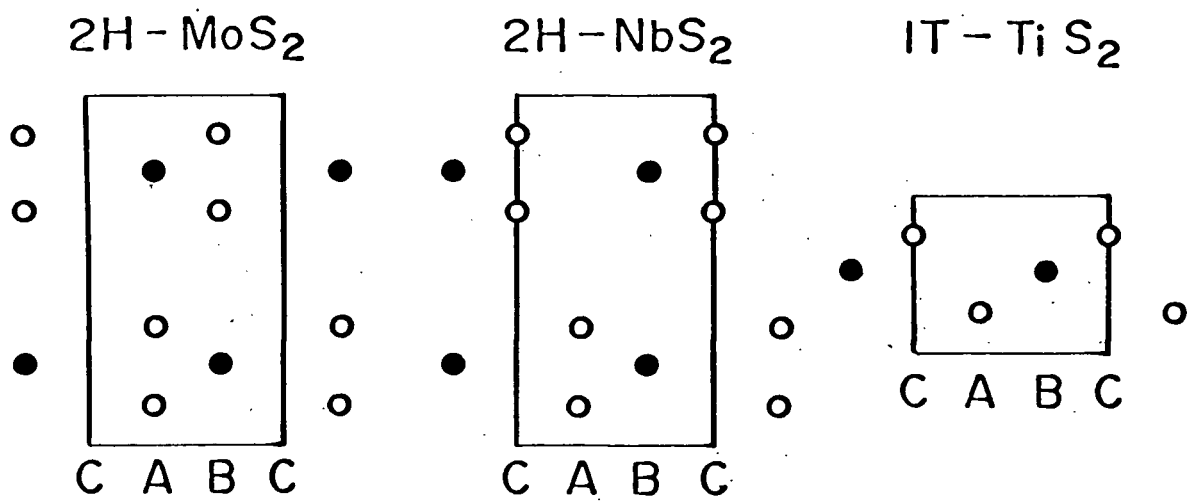

(b)

● = Metal

o = Chalcogenide

Fig. 2 - Common structures of the layered MX_2 compounds

a) 3-dimensional drawing

b) 110 sections (solid line outlines the unit cell)

(after Wilson and Yoffe 1969)

chalcogenide* atoms, X, in planes with an underlying hexagonal lattice. The crystal consists of stacks of these X-M-X planes.(Fig. 1) There are two possible sandwich structures (Fig. 1b), differing in how the chalcogenide atoms are arranged around the metal atoms. In the sandwich planes, there are three positions in the unit cell where atoms can lie, denoted A, B, and C. (X and M atom positions are represented by large and small letters respectively.) The trigonal prism coordination is thus denoted AbA, while the octahedral coordination is AbC. Complicated stacking sequences have been observed, but the most common structures are the simple ones illustrated in Fig. 2a. 2H-MoS_2 and 2H-NbS_2 type structures are similar in that they include two layers per unit cell and the chalcogenide coordination is trigonal prismatic. (The 2H- prefix means that the structure has 2 layers per unit cell with point group symmetry in the hexagonal division of the hexagonal system.) Both structures belong to the space group $P6_3/mmc\text{-}D^4_{6h}$. The two structures differ in their stacking sequence. 2H-MoS_2 stacks with alternate Mo atoms unaligned, while the Nb atoms are aligned in NbS_2.(Fig. 2b) Note that by sliding the sandwich planes in 2H-MoS_2 so that the Mo atoms align, the resulting structure is that of 2H-NbS_2. The other common stacking arrangement is that of 1T-TiS_2, which has octahedral coordination of the sulfur atoms in the sandwich planes. (The 1T- prefix stands for 1 layer per unit cell with point group symmetry in the trigonal division of the hexagonal system.) 1T-TiS_2 belongs to the space group $P\bar{3}m1\text{-}D^3_{3d}$. Like in NbS_2, the metal atoms in TiS_2 are all aligned.

Large anisotropies in mechanical and electrical properties exist between directions perpendicular and parallel to the sandwich layers.

---

* X can be either S,Se, or Te.

There is only weak Van der Waals bonding between sandwich layers as compared with the strong molecular X-M bonding in the sandwiches. It is possible to insert other atoms or molecules in the Van der Waals gaps between the molecular planes. This process is known as intercalation. There are two different types of sites for the intercalate in the sandwich gaps. A tetrahedral site lies at the centre of the tetrahedron formed by four surrounding chalcogenide atoms. Similarly, an octahedral site is located at the centre of the octahedron formed by six surrounding chalcogenide atoms. There are one octahedral and two tetrahedral sites per MX_2 molecular unit in the common structures shown in Fig. 2. In the MoS_2 structure, the octahedral sites are located at the C positions in Fig. 2b, while the tetrahedral sites are found at the A and B positions.

1.2 The MoS_2 battery

Our batteries consist of an MoS_2 cathode, a lithium metal anode, and non-aqueous electrolyte. Lithium is used because of its weight and because it diffuses rapidly in many structures. An electrolyte solution that doesn't react with lithium is required, hence the need for a non-aqueous solvent. The electrolyte used contained a lithium salt, either lithium perchlorate, $LiClO_4$, or lithium bromide, LiBr, dissolved in propylene carbonate liquid (PC), 1,2 propanediol carbonate.

The processes involved in a cell discharge are illustrated in Fig. 3. Lithium ions diffuse through the electrolyte to the MoS_2 cathode whereupon intercalation occurs. An equal number of ions must enter the solution at the anode. Electrons from the lithium metal provide the cell current and flow to the cathode via the external circuit, thus maintaining its overall

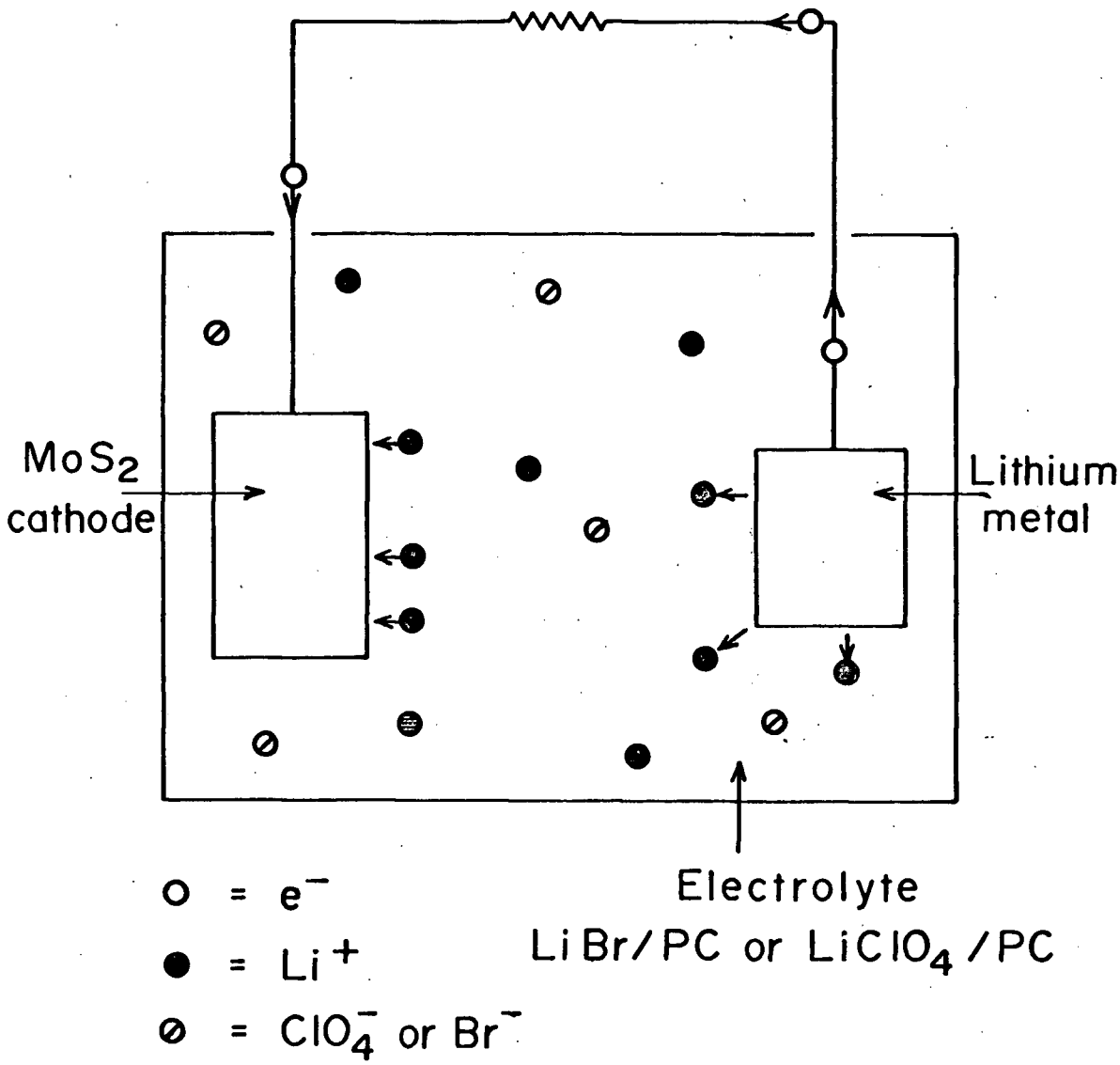

Fig. 3 - Processes involved in a discharge of the Li-MoS_2 system

neutrality. On a recharge, these processes occur in reverse with the lithium plating back on the anode.

The voltage of the Li-MoS_2 cell depends on the state of charge. Fig. 4 shows the voltage profile of a cell prepared as described in Sect. 3 and cycled at constant current. Initially, upon continuous discharge, the cell voltage follows the path ABCEF. Three different paths (BA,ECD, and FG) may be followed upon recharging, depending upon the starting point. The cell is not reversible along paths BC or EF. With these exceptions, subsequent cycling is permitted along any pathway. Thus the cell is capable of cycling in the three phases represented by the paths AB,DE, and GF on the voltage profile. These shall henceforth be referred to as phases 1,2, and 3 respectively.(Typical voltage profiles of cells cycling at constant current in these three phases appear in Fig. 5.) So a cell in phase 1 can be converted into phase 2, and a cell in phase 2 can be converted into phase 3. The reverse situation is not possible, at least at practical recharge rates (See Sect. 4). The transition from phase 1 to phase 2 begins at point B and ends at C. A battery discharged to a state midway between B and C appears to consist of a phase 1 and a phase 2 cell run in parallel. Similarly, the transition from phase 2 to phase 3 begins at E and ends at F. And,batteries discharged to a state midway between E and F act like a phase 2 and a phase 3 cell run in parallel.

Unfortunately, at the present time, accurate determination of the cathode's lithium content versus cell voltage has not been obtained. In Fig. 4, the values of x in the compound Li_xMoS_2 were determined from coulombic transfer. (ie. The amount of lithium present in a MoS_2 cathode of known weight was calculated on the assumption that one lithium atom

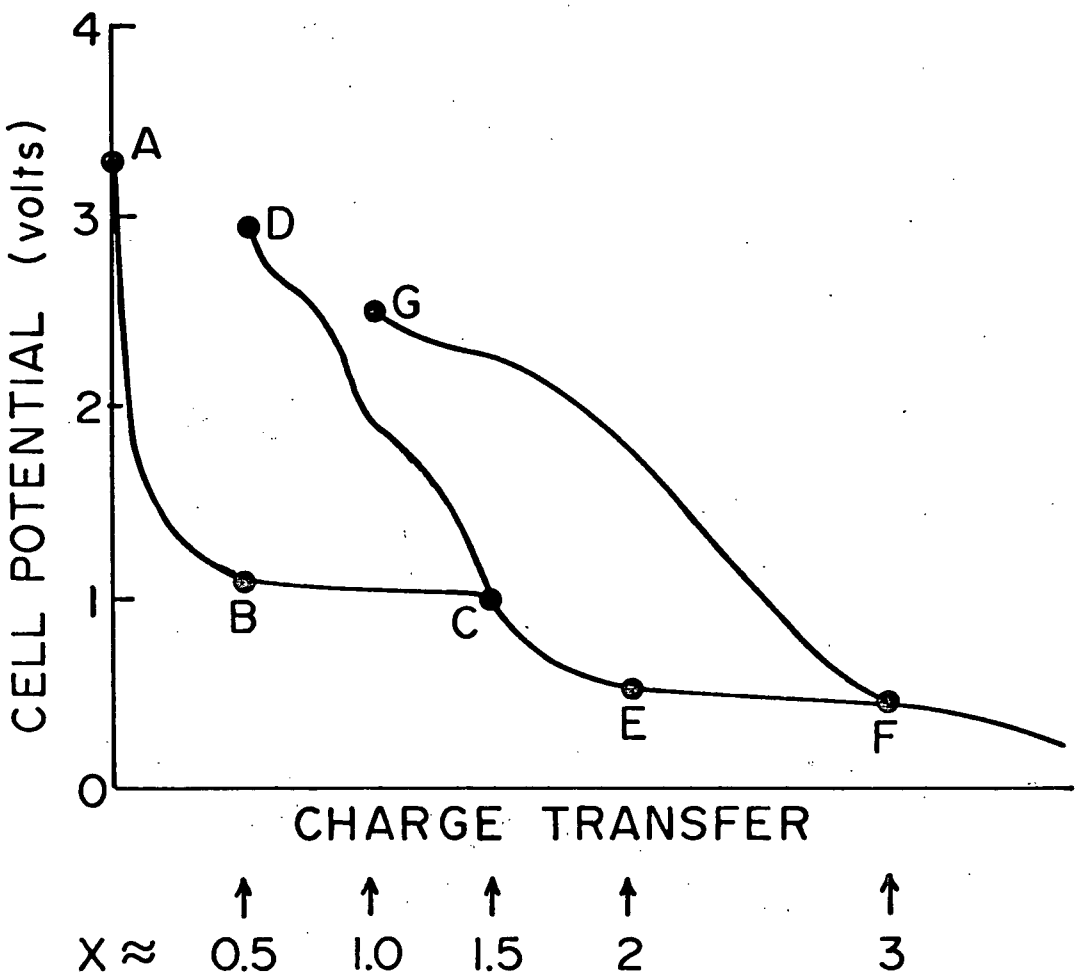

Fig. 4 - Voltage vs. charge transfer of a Li-MoS_2 battery (constant current)

This profile is representative of cells prepared and cycled as described in Section 3.

The values of x in the compound Li_xMoS_2 were determined from coulombic transfer.

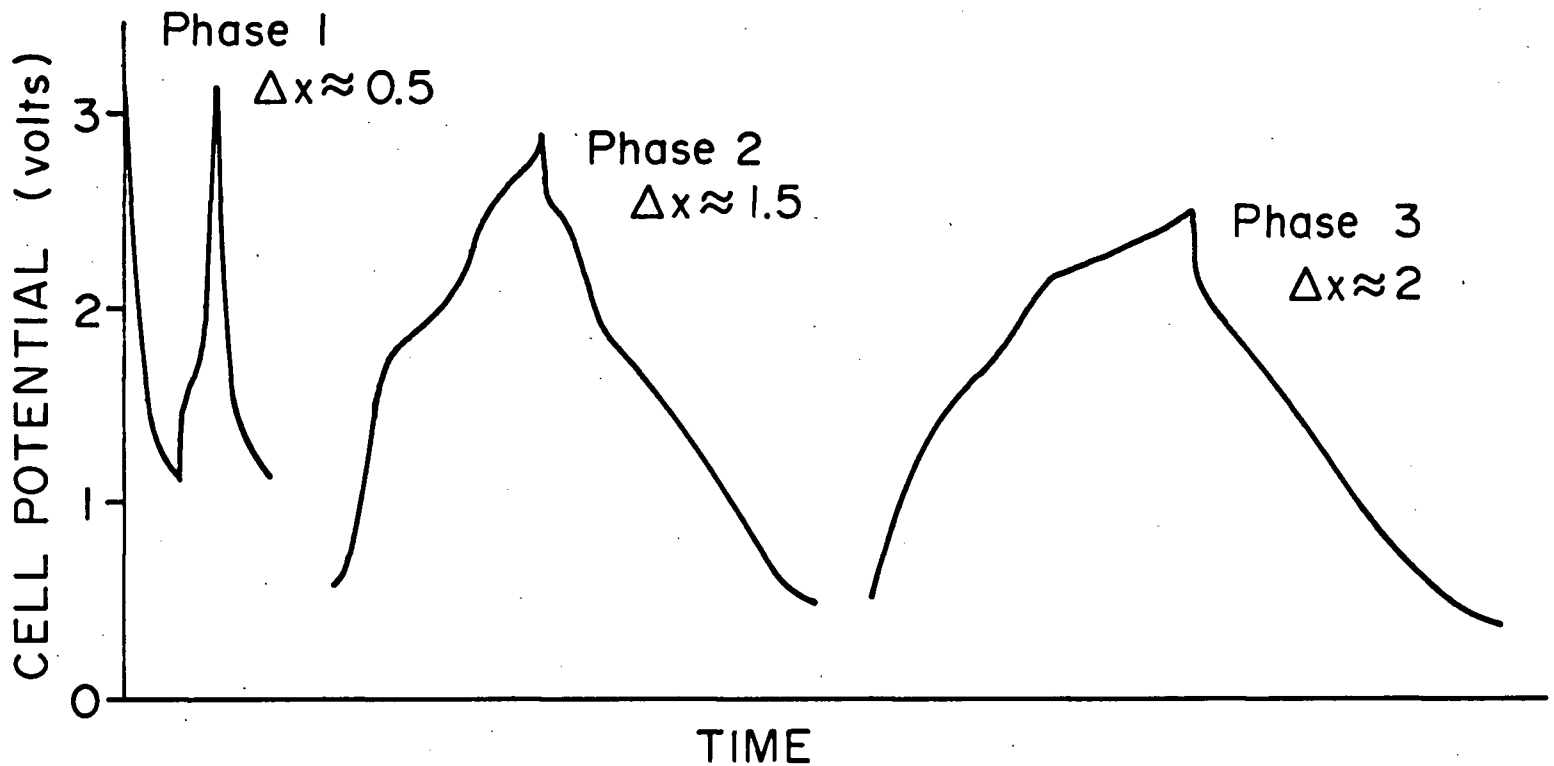

Fig. 5 - Voltage vs. time profiles of cells cycled in the three phases (constant current)

These plots were obtained from cells prepared and cycled as described in Section 3. (The difference in capacity between discharge and recharge is believed to be caused by a self-recharge process. See Section 3.)

intercalates per electronic charge transferred.) The possible presence of a side reaction (Sect. 3) introduces an uncertainty in these measurements.

2. X-ray Diffraction Theory

The unit cell dimensions and structure of the MoS_2 cathode in various stages of discharge were determined from powder X-ray diffraction patterns using the Debye-Scherrer method. The directions of the diffracted X-ray beams provide information on the shape and size of the unit cell, while their relative intensities depend on the arrangement of the atoms in the unit cell. In this section, basic theory pertinent to the experiment is presented. For further details, two good references are Klug (1974) and Cullity (1956).

2.1 Direction of the diffracted beam

The Bragg law illustrates how the angle of the diffracted X-ray beam depends on the distance between lattice planes of the crystal. The relation is

$$\sin \theta = \frac{\lambda}{2d} \qquad (2\text{-}1)$$

where θ = Bragg angle of scattering

λ = wavelength of the X-radiation

d = distance between lattice planes

Lattice planes are specified by their Miller indices (hkl). Crystallographers define these as " a set of integers with no common factors*, inversely proportional to the intercepts of the crystal plane along the

---

* Miller indices with a common factor represent an imaginary lattice plane. Higher order reflections from real crystal planes are thought of as being reflections from imaginary lattice planes.

crystal axes. " (Ashcroft and Mermin 1976) Some lattice planes in a hexagonal lattice are shown in Fig. 6.

Equations relating the distance d between adjacent lattice planes and their Miller indices can be derived from the lattice geometry. For example, hexagonal lattices obey

$$\frac{1}{d^2} = \frac{4}{3}\left(\frac{h^2+ hk + k^2}{a^2}\right) + \frac{l^2}{c^2} \qquad (2\text{-}2)$$

where a and c are lattice constants. Diffraction directions are usually specified by the d spacing of the lattice planes, since θ depends on the wavelength of the X-radiation used.

2.2 Intensity of the diffracted beams

X-ray patterns obtained using the Debye-Scherrer method are composed of diffraction lines. (See Fig. 8) Reflections from lattice planes of the same d spacing superimpose to form one diffraction line. This set of equivalent planes is represented by {hkl} where (hkl) are the Miller indices of any plane in the set. The number of planes in the set {hkl} equals the multiplicity factor, ρ, for that set. Thus the intensity of a {hkl} diffraction line is equal to ρ times the intensity of a line produced from a {hkl} plane.

The intensity of a (hkl) line is proportional to the square of the geometrical structure factor, F. F depends on the position and elemental type of the atoms in the unit cell. (See Ashcroft and Mermin 1976) Suppose the unit cell contains n atoms with fractional coordinates (u_j,v_j,w_j) relative to the crystallographic axes $\bar{a}$,$\bar{b}$, and $\bar{c}$. The geometrical structure factor, F_{hkl} associated with the (hkl) plane

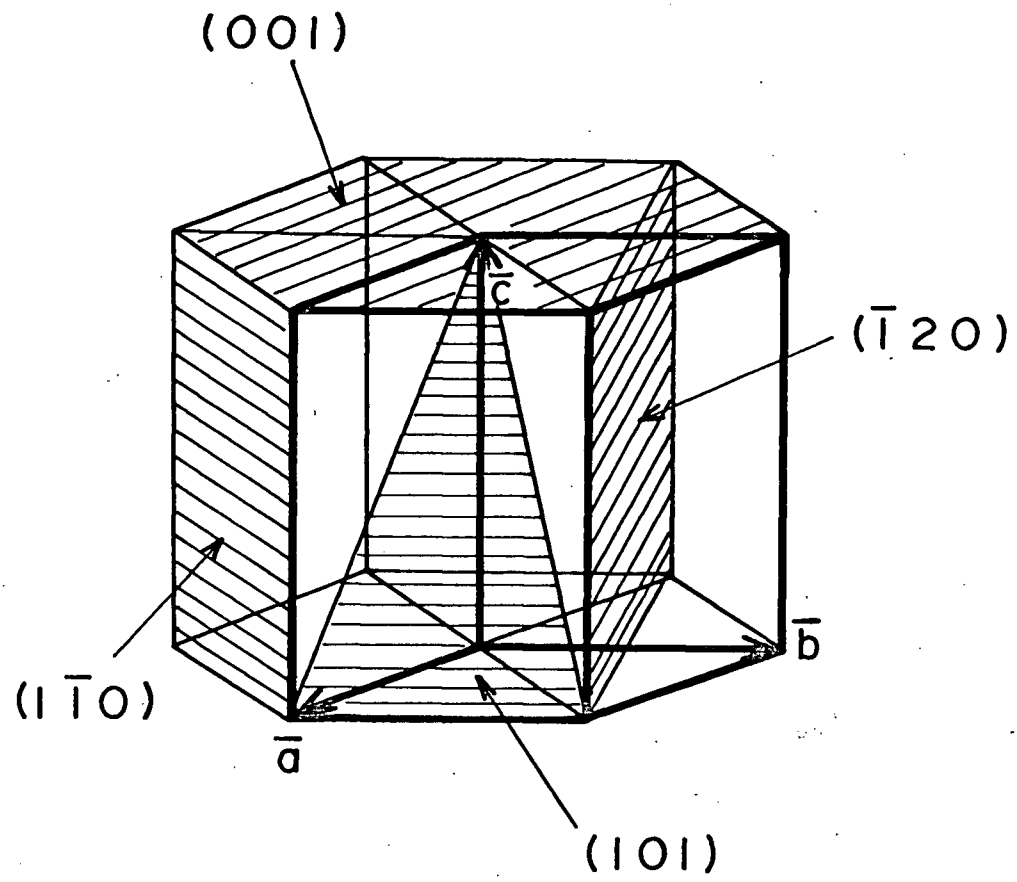

Fig. 6 - Some lattice planes (shaded) and their Miller indices in a hexagonal lattice. $\bar{a}$,$\bar{b}$, and $\bar{c}$ are the crystallographic axes defining the unit cell. In a hexagonal lattice,

$a = b \neq c$

Angle between $\bar{a}$ and $\bar{b}$ is 120°

$\bar{c}$ is perpendicular to the ab plane

Thus two parameters, a and c, describe the unit cell of a hexagonal lattice. (after Cullity 1956)

is given by

$$F_{hkl} = \sum_{j=1}^{n} f_j \, e^{i\,2\pi\,(hu_j + kv_j + lw_j)} \qquad (2\text{-}3)$$

where f_j is the atomic scattering factor of the jth atom. Values of f_j for the various elements were extrapolated from tables provided in Cullity (1956).

Calculations of the relative intensities of the diffraction lines were made according to the equation

$$I = |F|^2 \, \rho \left(\frac{1 + \cos^2 2\theta}{\sin^2\theta \, \cos\theta}\right) \qquad (2\text{-}4)$$

(For Debye-Scherrer method only)

where I = relative integrated intensity of the {hkl} line

F = geometrical structure factor of the (hkl) plane

ρ = multiplicity factor

θ = Bragg angle

The angular correction term in equation (2-4) is known as the Lorentz-polarization factor. An unpolarized beam introduces an angular dependence to the diffracted intensity proportional to $(1 + \cos^2 2\theta)$, the polarization factor. Other trigonometric factors, specific to the Debye-Scherrer method, introduce the $(\sin^2\theta \, \cos\theta)^{-1}$ dependence, the Lorentz factor.

Some corrections are not included since they are difficult to calculate. Absorption in the sample itself and thermal vibrations of the crystal's atoms will alter the observed intensities. These effects are not negligible and must be considered when comparing calculated intensities to experimental data. Both effects are relatively constant over small ranges in θ, so agreement between theory and experiment is generally deemed satisfactory if the observed relative intensities of

closely-neighboring lines fit the calculation. The relative observed intensities of two lines of large angular separation is not expected to agree well with calculations using equation (2-4).

2.3 Debye-Scherrer method

Powder X-ray patterns are obtained using a cylindrical camera as shown in Fig. 7. The specimen is rod-shaped and is mounted on the axis of the camera. The diameter of the specimen is kept below 0.3 mm so that the diffraction lines will not be too broad. The sample is usually rotated to increase the number of grain orientations presented to the X-ray beam. Film is mounted along the circumference of the camera. The diffracted beams come off the sample as a set of cones and create patterns as shown in Fig. 8.

The Bragg angle of each line is measured and converted to d values. To determine a new sample structure, first the unit cell is found by fitting d spacings of trial unit cells to those observed. Atomic arrangements are then similarly determined by fitting the calculated intensities of trial structures to the rough visual estimates made of the film line intensities. Similarities to known structures simplified the determination of the intercalated MoS_2 structures.

If their characteristic X-ray spectra are already known, other compounds can easily be identified by matching the patterns . Decomposition products present in the batteries were identified in this way.

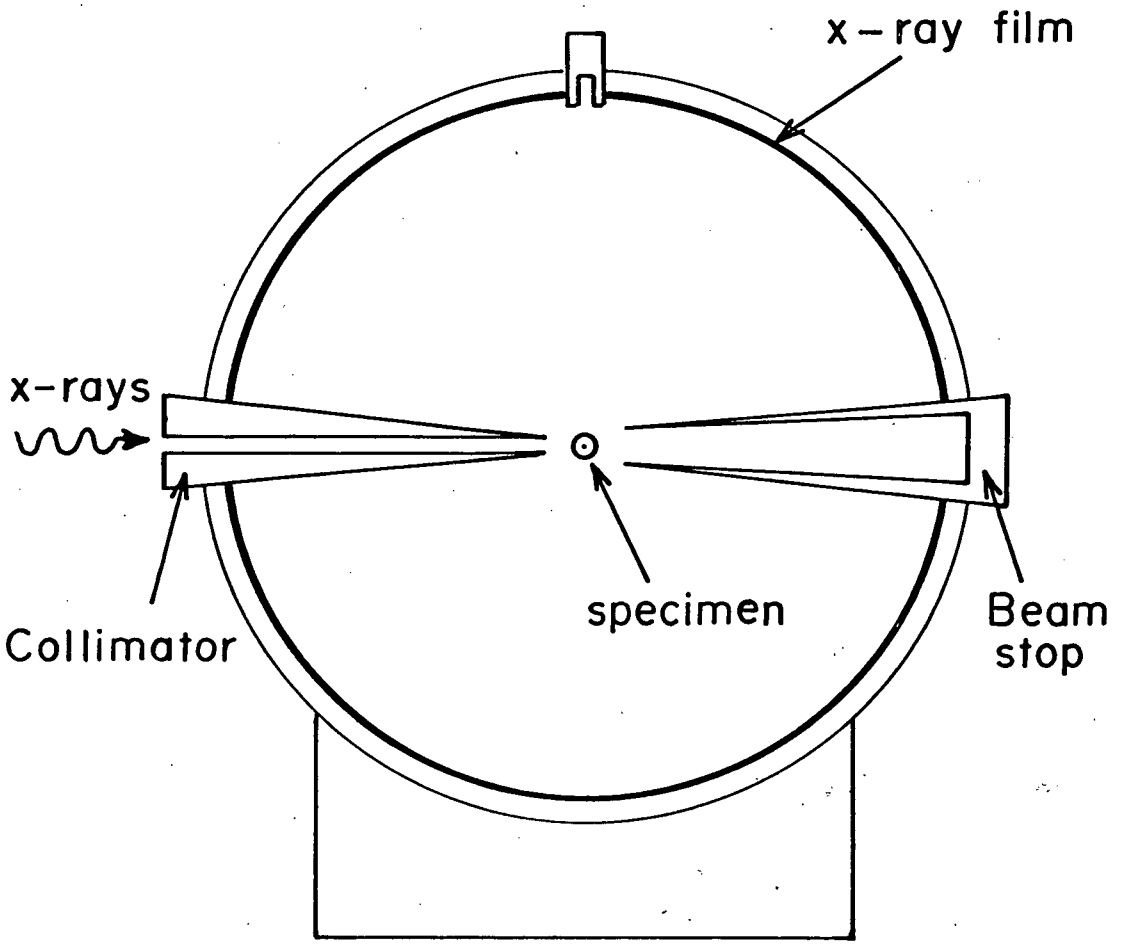

Fig. 7 - Debye-Scherrer camera (side view)

Specimen is rod-shaped, $\lesssim$ 1 cm long, < 0.3 mm in diameter. It is mounted and rotated on the axis of the camera.

Camera diameter = 114.83 mm

Entrance aperture is 1.0 mm in diameter.

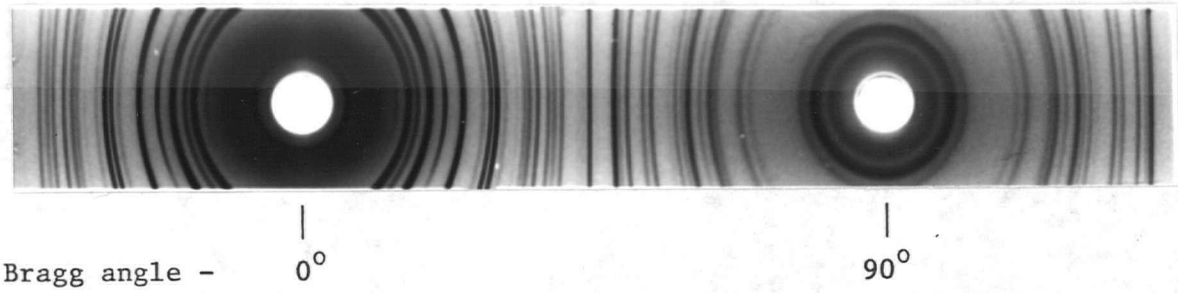

Fig. 8 - Debye-Scherrer picture of 2H-MoS_2

(Straumanis or unsymmetrical mounting of film)

3. Experimental Procedure

The study of the Li_xMoS_2 intercalation compounds by X-ray diffraction techniques is difficult because these materials are unstable in air and because a self-recharge mechanism is associated with their cathodic preparation. The instability of the Li_xMoS_2 compounds in air required that all steps involved in the preparation of the samples used in the X-ray studies be carried out in an inert atmosphere, and that the actual sample be sealed in a thin wall glass capillary.

A further difficulty arises due to the self recharge characteristics of the Li_xMoS_2 cathodes. Self-recharge refers to the tendency (observed in all cathodes studied) to show a rise in the open circuit voltage upon standing for a period of time. This voltage rise may result from an equilibrization of the (initially non-uniformly intercalated) lithium or it may arise from an unidentified side reaction at the cathode-electrolyte interface which results in a slow depletion of the intercalated lithium. It has proved impossible to avoid this difficulty and hence X-ray measurements had to be made immediately after the cathodic preparation of the sample. Many trial runs were necessary before an acceptable technique was developed and in total over 100 X-ray exposures were taken in support of the data presented in this thesis.

3.1 Cathode preparation

MoS_2 cathodes were prepared on aluminum or platinum foil substrates. Superfine MoS_2 powder suspended in oil* was baked onto the degreased

---

* Supplied by Molybond Laboratories, Australia

substrate for roughly 20 minutes at 575°C in a nitrogen gas flow. The oil comes off as vapor and is carried away by the nitrogen gas. It was found that baking at such high temperatures was necessary to remove the heaviest tars which otherwise coated the MoS_2 grains and prevented intercalation. Upon slow cooling (≈20 minutes), the MoS_2 adhered to platinum but not to aluminum substrates, presumably because of the greater thermal expansion of aluminum. In order to prevent peeling of the MoS_2 on aluminum substrates, the substrates were initially annealed for 20 minutes at 575°C and a small amount of oxygen gas was added to the nitrogen gas flow (Fig. 9). MoO_2 is formed (determined by X-ray analysis) by incomplete oxidation of the MoS_2. An MoO_2 coating of the MoS_2 grains has been found to be sufficient for good mechanical and electrical contact on aluminum substrates. Approximately 4 cm^2 of heavy duty aluminum foil (6 mg/cm^2) were coated per bake. Only about this much cathode material could be made at a time since MoO_2 formation was not uniform along the length of the preparation tube. The presence of small amounts of MoO_2 introduces complications in the analysis of X-ray data, but cathodes prepared on aluminum foil in this manner had a slower self-recharge rate than cathodes with platinum backing, especially at low cell potentials. Consequently, aluminum backed cathodes were used for all measurements taken at potentials < 2 volts. The ratio of MoO_2 to MoS_2 was generally ≈ 10-20% by weight*, certainly not negligible. To reduce

---

* Determined by rough visual comparisons of the relative intensities of X-ray line patterns of MoO_2-MoS_2 mixtures of known composition. The MoO_2 in these standard mixtures was present as individual grains, not as a coating of the MoS_2 grains. The grains are sufficiently small (≈1 micron) so that X-ray penetration is fairly uniform. Absorption of the diffracted beam in the grain will make the MoO_2 content of a coated grain appear too high according to the standard. But, MoO_2 also acts as a battery, and the weight of MoO_2 present can be determined from its capacity. MoO_2 content as measured by this method approximately agrees with that measured by X-rays. Apparently, absorption of X-rays under the grain surface is not significant.

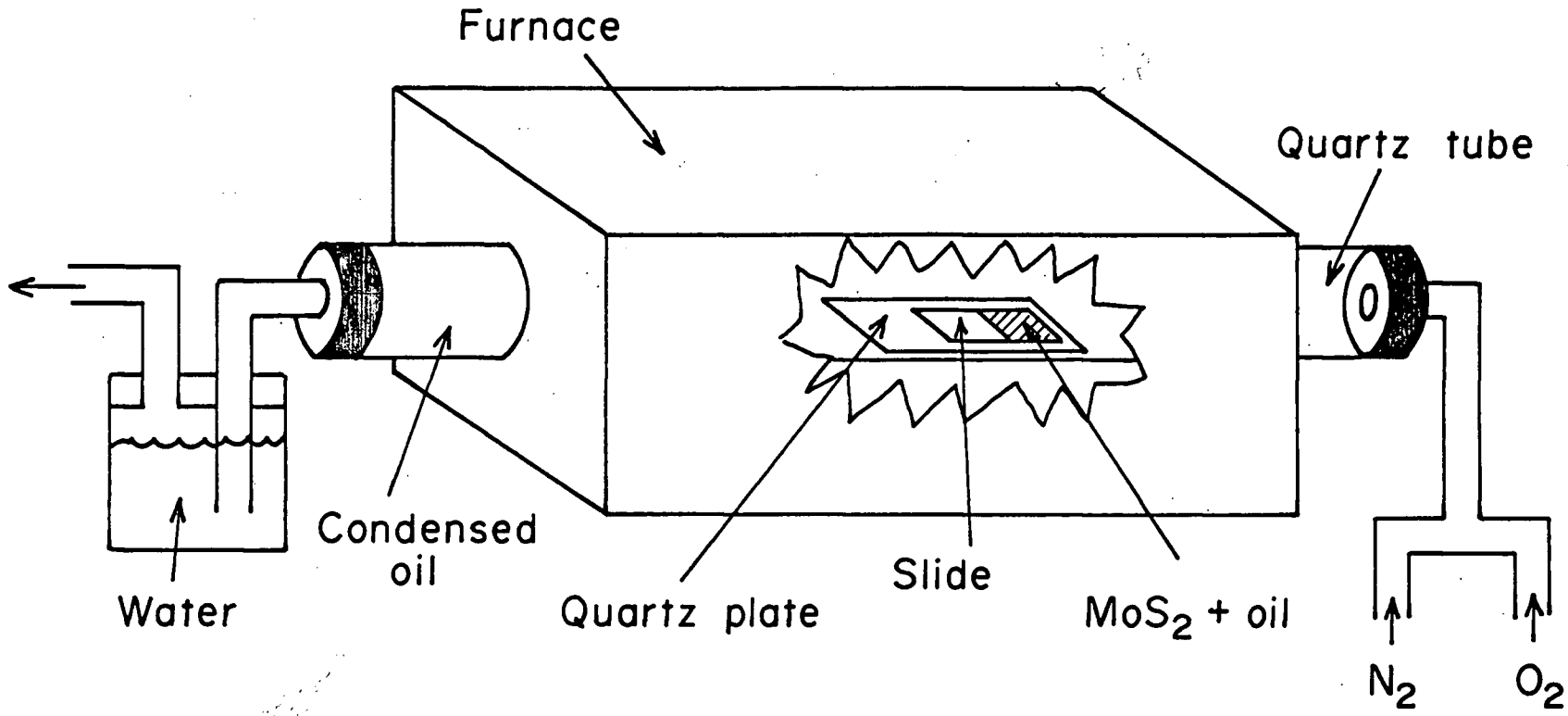

Fig. 9 - Apparatus used for cathode preparation on aluminum substrates. (Platinum backed cathodes were prepared in a similar fashion only no oxygen was used.)

Dimensions: glass slide - 3" x 1" x 1 mm
quartz plate - 4 cm x 15 cm x 6 mm
quartz tube - 115 cm long, 4.5 cm O.D., 4.15 cm I.D.
furnace - 80 cm long
distance from mixing point of N_2 + O_2 to quartz tube - 75 cm

Flow rates: N_2 - 800 cc/min.
O_2 - 0.2 cc/min. for the first 3 minutes of bake

inhomogeneity of the sample, thin layers of MoS_2 were applied on the substrate (0.3-0.5 mg/cm^2). Cathodes made in this way are quite porous with a density of ≈ 1.5 g/cm^3. The density of MoS_2 is 4.8 g/cm^3.

3.2 Cell construction

Cells were assembled in a Vacuum Atmospheres glove box under an argon atmosphere. (< 1 ppm water and oxygen was obtained by recirculating the box atmosphere through a Hydrox purifier.) Every cell contained two cathodes which were discharged in parallel. One was to be used for the X-ray sample, while its twin was used as a dummy in order to monitor the voltage rise indicative of the self-recharge. The substrate of each cathode was 2 x 1 cm^2 in size, with 1 cm^2 on one side coated with MoS_2. Thus each cathode held ≈ 0.3-0.5 mg of MoS_2. The twin cathodes were mounted as shown in Fig. 10, with the MoS_2 coated sides facing the lithium anode.

The anode consisted of lithium foil pressed onto a nickel screen. The electrolyte used was either a 1 M $LiClO_4$ in PC solution or a 0.7 M LiBr in PC solution. Both salts are hydroscopic so each was fuse dried (heated under vacuum until melted) to remove any water. The propylene carbonate (Eastman Kodak) was twice distilled under vacuum and was passed through several columns of molecular sieve and activated alumina to remove water and organic impurities. (Remaining amounts of impurity, notably glycol, are under suspicion as the cause of a self-recharging side reaction.) Solder connections to the electrodes were made to wires above the level of the electrolyte since the solder decomposed in the solution. The entire assembly is enclosed in a glass beaker (1½" diameter, 2" high)

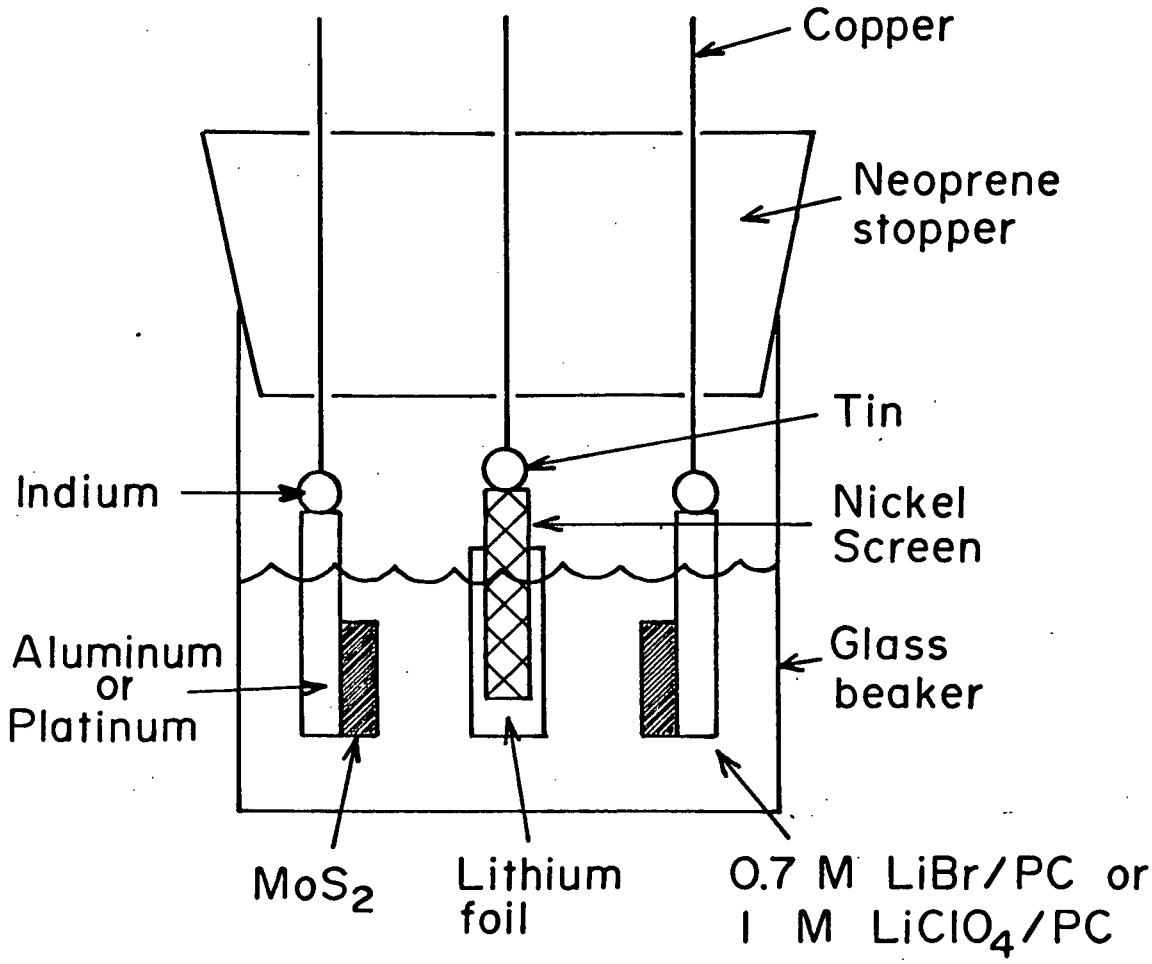

Fig. 10 - Twin cathode cell assembly (side view of electrodes)

with connections running through the neoprene stopper. (Black rubber stoppers react with PC and eventually crumble.)

3.3 X-ray specimen preparation

Cells were automatically cycled to the appropriate point on the discharge curve (Fig. 4) using a PAR coulometry cell system as a constant current supply. Each cathode was cycled at a constant current of 100 μA, thus the current density was always 100 $\mu A/cm^2$. In order to minimize any self-recharging, the X-ray analysis was performed as soon as possible after the end of the discharge. First, the twin cathodes were raised above the electrolyte level to minimize electrolyte contact with the cathodes. The cell was then transferred to the glove box. This involves pumping down the cell contents, but since PC has a low vapor pressure, the cathodes remained wetted with electrolyte. In the argon atmosphere, the MoS_2 on the test cathode was scraped off the substrate and onto a glass slide, giving one a puddle of intercalated MoS_2 and electrolyte. A tiny open-ended Pyrex tube (length $\leq$ 1 cm, wall thickness $\approx$ 0.02 mm, O.D. $\approx$ 0.2 mm) was used to seal the X-ray sample in an argon atmosphere. (Fig. 11) When dipped into the puddle, the tube loads itself with sample through capillary action. The tube is only partially filled with sample solution in order to allow the ends to be sealed with hard plasticine. It is necessary to start with a thick slurry of sample solution in order to reasonably fill the tube. After removal from the glove box, the sample tube is cleaned externally with acetone to remove the adhesive left behind from the scotch tape. (The tube is taped to a spatula for easy manipulation.) The salt LiBr or $LiClO_4$ is dissolved in PC and consequently does not contribute any diffraction

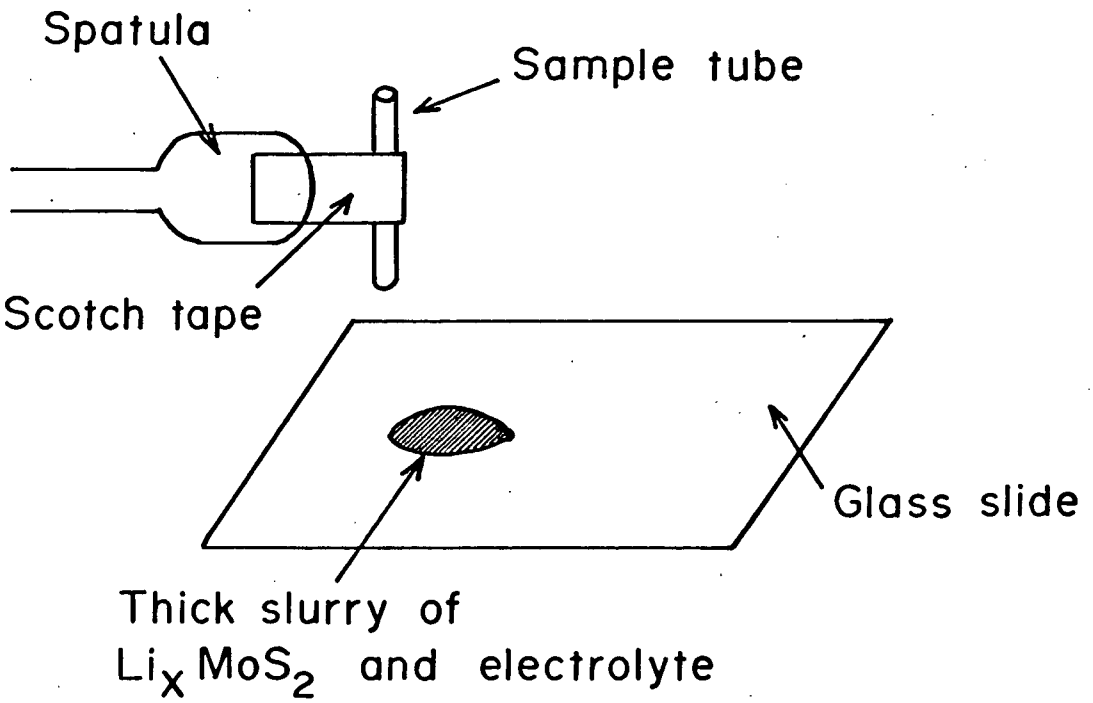

Fig. 11 - X-ray specimen preparation

lines. Some scattering of X-rays due to the glass can be seen. (Fig. 15)

3.4 X-ray procedure

The sealed specimen was centered in a 114.83 mm diameter Phillips Debye-Scherrer camera having a 1.0 mm entrance aperture. Copper Kα radiation (λ = 1.542 Å) was used at settings of 35 KV and 25 mA. The process of preparing the X-ray specimen takes roughly ½ hour mainly due to transit time into the glove box. The X-ray run lasts 1½ hours, so self-recharging times are limited to ≃ 2 hours. However, as will be seen, at the lowest voltages on the discharge curve, cathodes self-recharge so quickly that significant uncertainties are introduced in the measurements. The amount of self-recharge is determined by measuring the open circuit voltage of the dummy cathode when the X-ray run is finished. The dummy remains suspended above the electrolyte until this voltage is measured.

4. Results and Discussion

Diffraction patterns were taken at various points on the voltage profile in Fig. 4. Within experimental error, both phase 1 and 2 Li_xMoS_2 can be indexed to hexagonal lattices. The layer spacing (c/2 in a 2 layer unit cell) and the a axis in these phases have been measured versus cell voltage. The major structural change associated with the phase 1 → 2 transition has been identified. The phase 3 structure appears almost amorphous, probably due to non-uniform straining of the lattice. Also, some decomposition products of the cell have been discovered.

X-ray patterns representative of the various points on the voltage profile appear in Appendix A along with their measured line spectra. The X-rays should uniformly* penetrate the small (≃1 micron) cathode grains, implying that the data provided in these patterns applies to the bulk material and not just to the surface. Line broadening is apparent in phase 2 and especially in phase 3 patterns. The cause of this seems to be non-uniform straining of the lattice. Further discussion on line broadening appears in Appendix B. The uncertainties in the data due to this and other effects are examined in Appendix C.

---

* An example of X-ray penetration in a copper sample is given in Cullity (1956). Using unfiltered Cu radiation, 95% of the recorded information applies to a depth of 25 microns, but 50% of that information originates in the first 5 microns. The linear absorption coefficients of Cu Kα radiation in Cu and Mo are ≃ 470 and ≃ 1670 cm^{-1} respectively. Thus similar penetration is expected in ≃ 1.5 microns of Mo as in ≃ 5 microns of Cu.

4.1 Phase 1 (A - B in Fig. 4)

2H-MoS_2 is hexagonal with c and a axes of 2 x 6.15 Å and 3.16 Å respectively. The sandwich height is 3.19 Å and the Van der Waals gap height is 2.96 Å (See Figs. 1 and 2). Cathodes of cells cycled in phase 1 visually appear no different than ordinary MoS_2, remaining gray in colour. X-ray spectra of discharged phase 1 cells (Fig. 15a) are identical to that of 2H-MoS_2. However, the fact that cells can be cycled in phase 1 implies that lithium must be going to the cathode. It is unlikely that the lithium is merely coating the MoS_2 grains since this would result in a cell voltage of approximately zero volts. Moreover, a coating corresponding to $x \simeq 0.5$ worth of lithium would be quite thick and should be detectable even visually. Lithium probably intercalates even in phase 1, perhaps just in a surface layer. It would seem unlikely that the X-ray spectrum would remain unchanged if the bulk material were intercalated with so much lithium. For example, the spectra of VS_2 and $Li_{0.33}VS_2$ are quite different (D.W. Murphy, C. Cros, et al 1977). However, the octahedral sites in the sandwich gaps should be roughly large enough to accomodate lithium ions*. It may be possible then to fill $\simeq \frac{1}{2}$ of the octahedral sites without significantly distorting the lattice. Another possibility is that the lithium is concentrated just beneath the surface of the MoS_2 grains. Such a thin shell could go undetected in a diffraction pattern.

---

* Assuming that the sulfur atoms in a sandwich are close-packed spheres, the octahedral sites in 2H-MoS_2 are large enough to accomodate a sphere of radius 0.77 Å. The radius of a lithium ion as given in the Handbook of Chemistry and Physics (1969) is 0.68 Å. A similar calculation implies that the tetrahedral sites are too small, being able to accomodate spheres of radius 0.46 Å.

4.2 Phase 1 → 2 transition (B - C in Fig. 4)

A colour and structure change are associated with this transition. The cathode turns from gray to black and from a phase 1 to a phase 2 type structure. Phase 2 Li_xMoS_2 is believed to be either a 2H-NbS_2 or a 1T-TiS_2 type structure.

The phase 2 spectrum at point C in Fig. 4 fits that of a hexagonal lattice with c = 6.33 Å and a = 3.34 Å. The possibility that c is some greater multiple of 6.33 Å cannot be ruled out from the present data, but no lines have been seen that would require a larger unit cell. Intensity calculations of a MoS_2 layer compound with these parameters and the common stacking sequences appear in Appendix D. The observed line intensities fit structures where the Mo atoms stack on top of each other. The NbS_2 and TiS_2 structures, with stacking sequences of /AbA CbC/ and /AbC/ respectively, are the most likely candidates*. (The quality of the X-ray patterns is too poor to identify the sulfur atom coordination or the number of layers per unit cell. For example, if the structure is similar to 2H-NbS_2, the {101} diffraction line should be relatively strong. No such line is seen. But, theory predicts it should be fainter than its two close neighbours, {100} and {102}. A broad {101} line may be washed out by its stronger near neighbours. An idea of the agreement that can be expected with a sharp diffraction picture is illustrated with the observed and calculated line intensities of 2H-MoS_2 in Appendix D.)

The NbS_2 structure can be obtained from the MoS_2 structure by shifting

---

* More complicated stacking sequences, with some layers octahedrally coordinated and some trigonally coordinated, have been reported in the literature (Wilson and Yoffe 1969), but are not as common.

the sandwich layers by $\frac{a}{\sqrt{3}}$, so that the Mo atoms align. A transition to the TiS_2 structure would also require reordering the sandwich layers themselves. (Landuyt et al (1976) postulate that in TaS_2 a sulfur plane can slip with respect to the host sandwich layer.) Intuitively the NbS_2 structure might seem more likely for phase 2 since less rearrangement of the crystal lattice is required. However, transitions from 2H-MoS_2 type → 1T-TiS_2 type structures have been reported in the literature (Landuyt et al 1976) as have 2H-MoS_2 type → 2H-NbS_2 type structural transitions. The austenite to martensite transition in steel also involves shifts of lattice planes, as the crystal structure goes from face-centered cubic to body-centered cubic (Robert E. Reed-Hill 1973). Line broadening is a common feature associated with this transition. Uniform and non-uniform stresses exist in the steel; the former causing shifts in the diffraction line positions, and the latter causing line broadening.

X-ray spectra taken at points along BC show a mixture of the two phases, dominated by the sharp, strong lines of phase 1. Generally only the 6.33 Å line of phase 2 shows up clearly, and it overlaps the 6.15 Å ({002}) line of phase 1 creating what appears to be a very broad line centered at ≃ 6.24 Å (Fig. 15b). Close to point C in Fig. 4, traces of other broad phase 2 lines become visible.

The phase 1 → 2 transition is reversible, but only at slow recharge rates. This may be due to poor lithium diffusion in the sandwich gaps near point D (Fig. 4) in phase 2. The unit cell here is much smaller than elsewhere in phase 2 (See Sect. 4.3) presumably with a much smaller sandwich gap. Trickle charging converts a phase 2 cell from point D to a strained version of a phase 1 cathode. X-ray spectra taken of these

reconverted cathodes resemble slightly strained 2H-MoS_2 (Fig. 15i). The line broadening seen in phase 2 is much reduced after the reverse transition, but the pattern is still not as distinct as that of the original 2H-MoS_2. A subsequent discharge of such a cathode reveals a plateau-like feature in the voltage profile, similar to the BC plateau in Fig. 4, except that it occurs at a higher voltage ($\simeq$ 1.4 V). At the end of this plateau-like feature, the cell has converted back into phase 2.

4.3 Phase 2 (D - C - E in Fig. 4)

Structural changes of Li_xMoS_2 appear to be fairly symmetrical over a cycle in phase 2. Changes occur in the size and apparently also in the positions of atoms in the unit cell of a cathode run in phase 2. Possibly even the shape of the unit cell is altered.

There are two kinks in the phase 2 voltage profile (Fig. 4), one at $\simeq$ 2 V and the other at $\simeq$ 2.7 V. X-ray spectra of cathodes run between the kink at 2 V and point E (0.5 V) are similar, with differences arising only because of small changes in the c and a axes of the unit cell. Between the two voltage kinks (2 V to 2.7 V), an extra faint line appears in the X-ray patterns. Assuming a 2 layer unit cell, this line can be indexed as {105}. Between point D and the upper voltage kink (3 V to 2.7 V), this line is no longer present. However, another faint line appears in the spectrum. Again assuming a 2 layer unit cell, this line can be indexed as {103}. Also in this pattern, the relative intensity of the {100} line to the {102} has increased to the point where they are visually equally strong.

1T-TiS_2 type structures have only one layer per unit cell. These extra lines cannot be fitted to such a structure. 2H-NbS_2 type structures with lattice parameters in the appropriate range are expected to have very faint

{103} and {105} lines. (See calculated pattern in Appendix D.) Also, the {100} line is expected to be significantly fainter than the {102} line. However, strong {103} and {105} lines are characteristic of structures with alternate Mo atoms aligned, sucn as 2H-MoS_2. And in such structures, the {100} line is expected to be more intense than the {102}. Finally, a {106} line is expected to be seen in 2H-NbS_2 type structures but is not evident in the X-ray pictures. However, this line would be located so as to overlap the phase 2 {110} line or the 1.71 Å MoO_2 line throughout most of phase 2. Near point D, though, the {106} reflection should be sufficiently clear of these other lines, and it is not seen. Faint {106} lines are characteristic of 2H-MoS_2 type structures. It seems likely then that as the cell is recharged in phase 2, the cathode is trying to revert from a NbS_2 type structure to its original structure. A decrease in the amount of non-uniform strain is also evident upon recharging, as the sharpness and number of lines in the X-ray patterns increase.

Within experimental error, phase 2 Li_xMoS_2 can be indexed to hexagonal lattices. It is possible that the shape of the unit cell is slightly distorted. For example, VS_2 is hexagonal and has a structure similar to 1T-TiS_2. D.W. Murphy, C. Cros, et al (1977) have discovered two different monoclinic phases of Li_xVS_2, α and β, occuring in ranges near x = 0.33 and x = 0.5 respectively. Both monoclinic phases are nearly hexagonal. Possibly our Li_xMoS_2 system is similar. The phase 2 spectra with the extra lines may be indicative of phases with different lattice systems.

On the assumption that the unit cell remains hexagonal throughout phase 2, the layer spacing (c/2 in a 2 layer unit cell) and the a axis have been plotted versus the phase 2 voltage profile in Fig. 12 and versus cell voltage in Fig. 13. (An explanation of the experimental

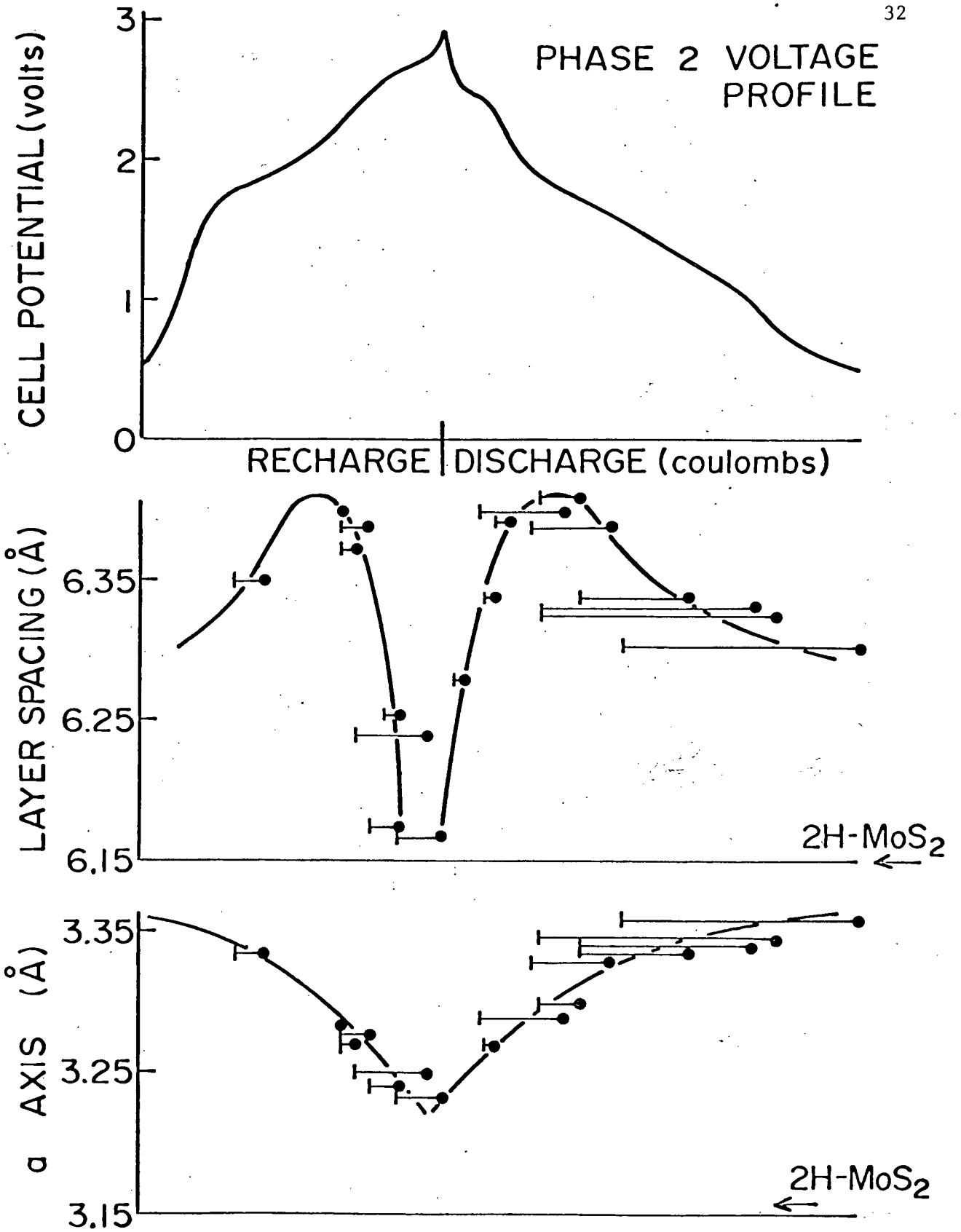

Fig. 12 - Layer spacing and a axis plots vs. phase 2 voltage profile (a axis sometimes not available with corresponding layer spacing)

Vertical error : layer spacing ± 0.03 Å, a axis ± 0.02 Å

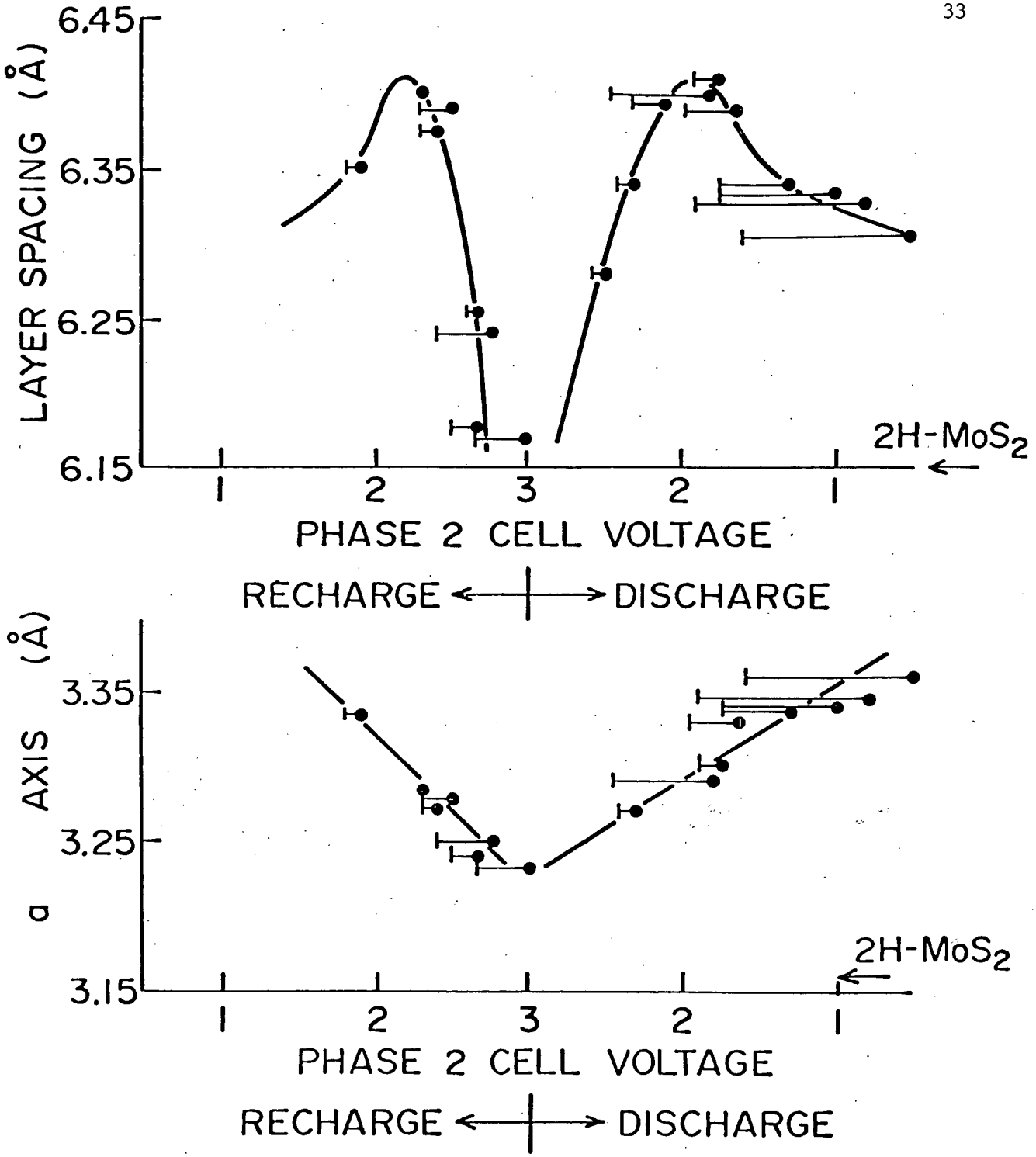

Fig. 13 - Layer spacing and a axis plots vs. phase 2 cell voltage (a axis sometimes not available with corresponding layer spacing)

Vertical error : layer spacing ± 0.03 Å, a axis ± 0.02 Å

uncertainties is given in Appendix C.) There is a maximum in the layer spacing, ≃ 6.40 Å, occuring at cell voltages near the kink in the voltage profile at 2 V. Coulombic transfer implies a chemical composition of Li_1MoS_2 at this point. This agrees with Whittingham (1975), who determined that the c axis in Li_1MoS_2 is some multiple of 6.40 Å. There is a sharp decrease in the layer spacing above 2 V. At the top of phase 2 (point D in Fig. 4), the layer spacing has approximately returned to its original phase 1 value. Below 2 V, the decrease is not as drastic, reaching a minimum of ≃ 6.30 Å at the low voltage end of phase 2. (This behaviour has been noted in other systems. For example, in TiS_2, the c axis is also seen to decrease with increasing amounts of intercalate. For the intercalated compounds Rb_xTiS_2 and Cs_xTiS_2, c decreases for $x > 0.42$ and $x > 0.56$ respectively (J.Bichon et al 1973)). The a axis, on the other hand, increases monotonically with the amount of intercalate. It definitely does not return to its original phase 1 value at the top of phase 2. (Confirmed by the displaced {110} line.)

There may be discontinuities in the variation of the layer spacing and a axis with cell voltage. However, due to the experimental uncertainty, more statistics or better resolution are necessary to confirm this. Abrupt changes in the unit cell size may be associated with the kinks in the voltage profile.

Plots of the layer spacing x a^2 and layer spacing/a versus the phase 2 voltage profile appear in Figs. 14a and b respectively. Assuming a hexagonal unit cell, the volume of the unit cell is given by $\frac{\sqrt{3}}{2}$ x the layer spacing x a^2 x number of layers per unit cell. It would appear from Fig. 14a that the unit cell volume gradually increases with increasing amount of intercalate. At the bottom of phase 2 (point E in Fig. 4), the

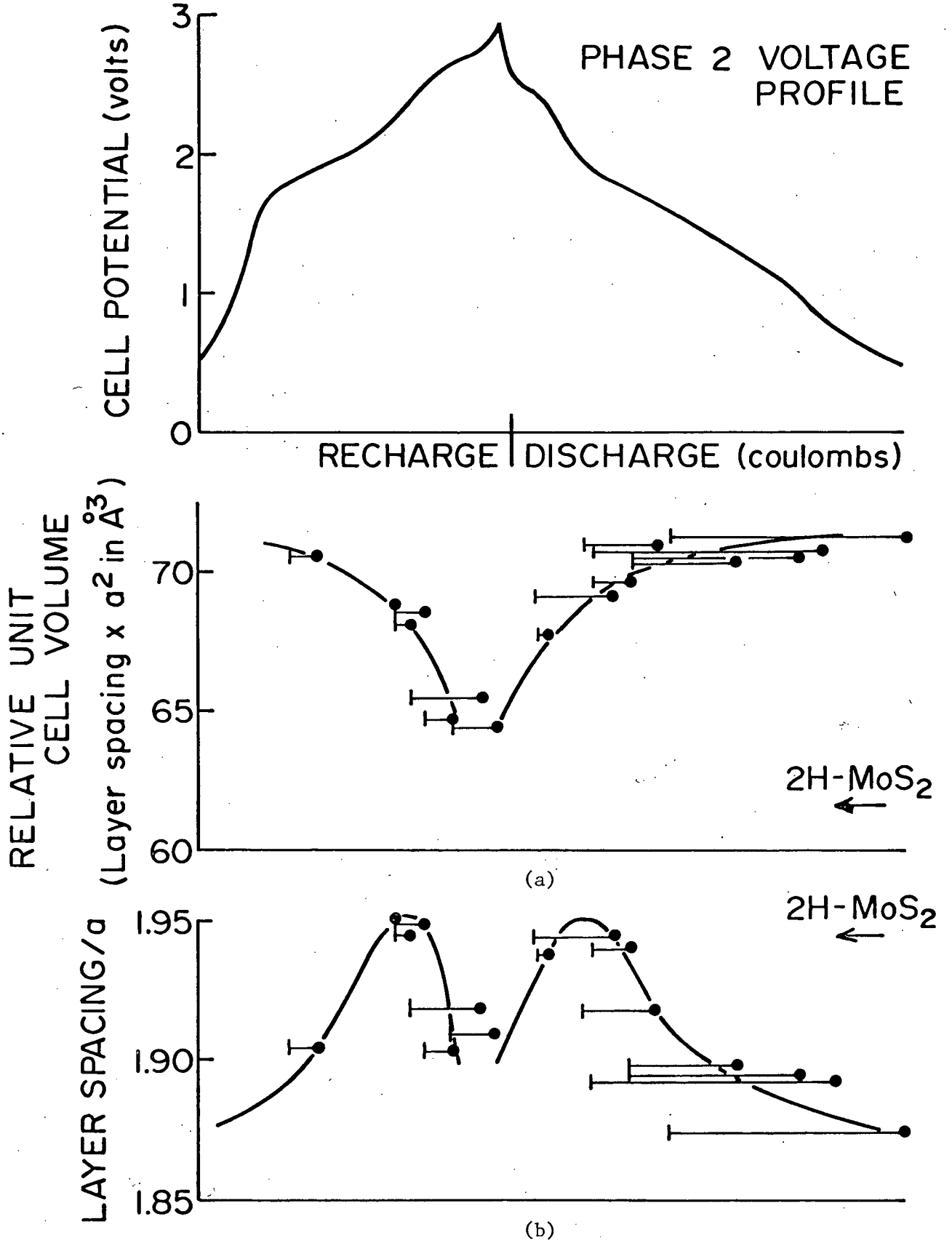

Fig. 14 - a) Relative unit cell volume and b) Layer spacing/a plots vs. phase 2 voltage profile

Vertical error : layer spacing ± 0.03 Å, a axis ± 0.02 Å

cathode volume has apparently increased by 15% over its original value. The minimum phase 2 volume remains a few per cent larger than that of the original 2H-MoS_2. The layer spacing /a ratio in phase 2 is never too far removed from the 2H-MoS_2 value of 1.945. There is a peak in the curve occuring near where the layer spacing itself is a maximum.

4.4 Phase 2 → 3 transition (E - F in Fig. 4) and Phase 3 (C - F in Fig. 4)

X-ray spectra of phase 3 cathodes appear almost amorphous (Fig. 15h). Only one very broad band at a low Bragg angle is ever visible. This band extends from a d spacing of ≃ 6.3 Å to ≃ 12 Å (the limit of the film). The featureless pattern may be due to the presence of severe non-uniform strains in the crystal lattice.(See Appendix B).X-ray spectra taken at points along EF still exhibit the phase 2 spectrum of point E. So far, no reversal of the transition has been observed in the diffraction patterns. Cells may have reached their maximum capacity at point F. Here, enough lithium (x = 3) has been intercalated to fill all the sites in the sandwich gaps.

4.5 Decomposition products

Discharged cathodes are unstable in air, presumably* forming hydrated complexes similar to those in the Li-TiS_2 system studied by Whittingham

---

* X-ray spectra of discharged cathodes exposed to air were similar to that of a cathode washed in water.

(1974). X-ray patterns of such cathodes upon exposure to air bore similarities to those of hydrated Li_xTiS_2. Occasionally the compound Li_2MoO_4 was also present, but only in those more deeply discharged samples, where presumably the lithium content was now high enough to allow Li_2MoO_4 formation.

There is also evidence of Li_2S formation in cathodes discharged into phase 3. In some X-ray patterns, two lines have been seen which fit the two strongest lines of the Li_2S spectrum. The formation of Li_2S is a possibility according to free energy considerations. All cathodes in phase 2 or 3 smell of H_2S upon exposure to air. This, however, may be due to decomposition of the cathode to Li_2MoO_4 and not the decomposition of Li_2S.

5. Summary

The MoS_2 cathode undergoes two phase transitions upon discharging. In the first transition, the sandwich layers shift such that the Mo atoms stack above one another. A rearrangement of atoms in the layers themselves is also a possibility. After the transition, the crystal lattice is subject to non-uniform stresses which diminish as lithium is removed. This first transition is reversible to some degree. The original lattice structure is regained, but with some non-uniform straining present. Little is known about the processes involved in the second transition, since the phase 3 structure appears almost amorphous. The transition may involve greater straining of the crystal lattice.

In the powder photographs, phase 1 cathodes always resemble 2H-MoS_2, while phase 3 cathodes seem almost amorphous. The unit cell in phase 2, however, is seen to vary throughout a cycle implying that intercalation takes place. The intercalation process appears completely reversible, since X-ray spectra taken at corresponding points on the discharge and recharge voltage curves are identical. The layer spacing reaches a maximum in the middle of the phase whereas the a axis increases monotonically with discharge. Discontinuities, corresponding to the kinks in the voltage profile, may exist in both the layer spacing and the a axis. The volume of the unit cell (proportional to the product - layer spacing x a^2) gradually increases with increasing lithium content to reach a maximum value that is 15% larger than the original. The minimum phase 2 value is still a few per cent larger than the original MoS_2, because although the layer spacing appears to return to its original value, the a axis remains

somewhat larger than before.

Unless exposed to air, no decomposition of phase 2 cathodes is evident in the X-ray patterns. Phase 3 cathodes may decompose to form Li_2S.

Bibliography

Ashcroft, N.W., and Mermin, N.D. 1976. Solid State Physics, Holt, Rinehart, and Winston, New York.

Bichon, J., Danot, M., et Rouxel, J. 1973. C.R. Acad. Sc. Paris, 276, 1283.

Chianelli, R.R. 1976. Journal of Crystal Growth, 34, 239.

Cullity, B.D. 1956. Elements of X-ray Diffraction, Addison-Wesley, Reading.

Klug, H.P., and Alexander, L. 1974. X-ray Diffraction Procedures for Polycrystalline and Amorphous Materials, 2nd Edition, J. Wiley & Sons, New York.

Landuyt, J. Van, Tendeloo, G. Van, and Amelinckx, S. 1976. Phys. Stat. Sol., A 36, 757.

McClune, W.F. 1977. Powder Diffraction File, JCPDS International Centre for Diffraction Data, Swarthmore.

Murphy, D.W., Carides, J.N., DiSalvo, F.J., Cros, C., and Waszczak, J.V. 1977. Mat. Res. Bull., 12, 825.

Murphy, D.W., Cros, C., DiSalvo, F.J., and Waszczak, J.V. 1977. Inorg. Chem., Vol. 16, No. 12, 3027.

Reed-Hill, Robert E. 1973. Physical Mettalurgy Principles, 2nd Edition, D. Van Nostrand Co., Princeton.

Schafhäutl, C. 1841. J. Prakt. Chem., 21, 129.

Weast, R.C. 1969. Handbook of Chemistry and Physics, 50th Edition, The Chemical Rubber Co., Cleveland.

Whittingham, M.S. 1974. Mat. Res. Bull., 9, 1681.

Whittingham, M.S., and Gamble Jr., F.R. 1975. Mat. Res. Bull., 10, 363.

Whittingham, M.S. 1976. J. Electrochem. Soc., 123, 315.

Wilson, J.A., and Yoffe, A.D. 1969. Advances in Physics, 18, 193.

Appendix A

Examples of X-ray spectra

X-ray patterns representative of the various points on the cell voltage profile appear in Fig. 15. Common to all the pictures is a diffuse band in the forward scatter region. This is caused by X-rays scattering off the glass specimen container. Also present in the patterns are line spectra of various Li_xMoO_2 compounds. (These spectra all exhibit sharp diffraction lines, making them easily distinguishable from phase 2 and 3 patterns.) Those Li_xMoO_2 spectra showing up in the patterns in Fig. 15 are presented in Fig. 16. The measured line spectra from all these pictures are also presented in this Appendix.

Ten X-ray patterns are shown in Fig. 15, and they are-

a) Phase 1 (discharged to 1.1 V)

b) Phase 1 → 2 transition (discharged to a point near C in Fig. 4 at 1 V)

c) Phase 2 (recharged to 2.65 V)

d) Phase 2 (recharged to 2.3 V)

e) Phase 2 (discharged to 0.8 V)

f) Phase 2 (discharged to 0.5 V)

g) Phase 2 → 3 transition (cycled in phase 3; incomplete transition from phase 2 → 3)

h) Phase 3 (cycled in phase 3)

i) Phase 2 → 1 transition (by self-recharging)

j) Phase 2 → ? (phase 2 cell washed in methanol)

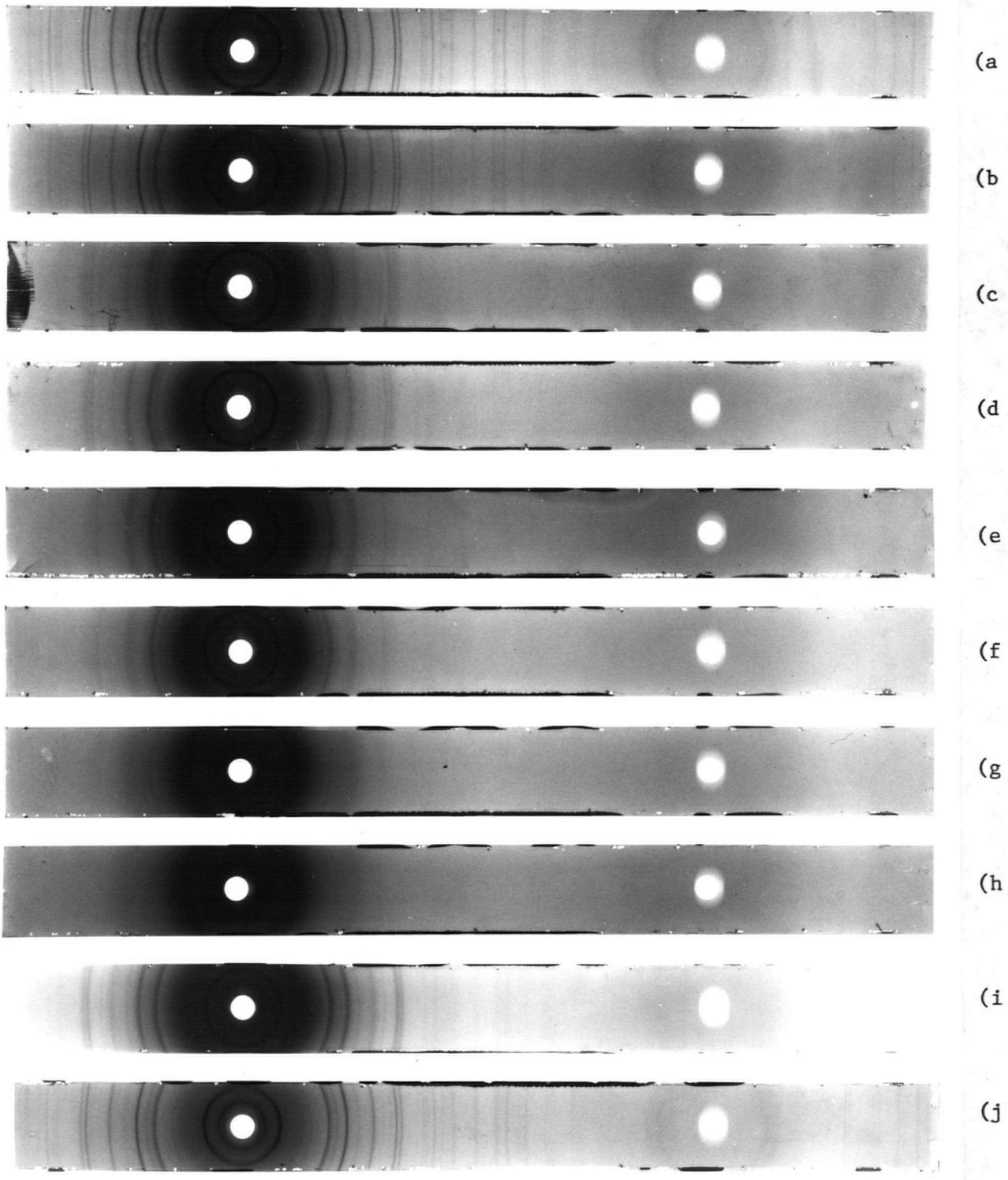

Fig. 15 - X-ray pictures of MoS_2 cathodes at various stages of discharge

(See Text)

The line spectrum of 2H-MoS_2 (see Fig. 8) as determined by the National Bureau of Standards is given in Table 1.

Table 1

Line spectrum of 2H-MoS_2

I	d (Å)	{hkl}
100	6.15	002
4	3.075	004
16	2.737	100
9	2.674	101
8	2.501	102
45	2.277	103
14	2.049	006
25	1.830	105
4	1.641	106
11	1.581	110
12	1.538	008,112*
2	1.4784	107
2	1.3688	200
4	1.3401	108
5	1.2983	203
4	1.2513	116
2	1.2295	0010
1	1.2224	109
4	1.1960	205

etc.

* The {112} index was not printed on the PDF data card (McClune 1977).

The following data was determined from the pictures in Fig. 15. The observed intensities given are visual estimates of the relative line strengths. In the following tables,

VS = Very Strong
S = Strong
M = Moderate
F = Faint
VF = Very Faint

All values of d are given in Å. The calculated d spacings were determined assuming the crystal lattice remained hexagonal. (See Sect. 2 for theory.)

Table 2

Line spectra of MoS_2 cathode patterns in Fig. 15

a) Phase 1

$I_{obs.}$	$d_{obs.}$	Identification
VS	6.17	{002}
F	3.56	Li_xMoO_2 (see Fig. 16c)
S	2.74	{100}
M	2.68	{101}
M	2.51	{102}
F	2.35	Aluminum
S	2.28	{103}

Remaining lines are those of 2H-MoS_2.

Some substrate can be scraped off while preparing the X-ray specimen. Aluminum lines were quite common in the spectra.

b) Phase 1 → 2 transition

$I_{obs.}$	$d_{obs.}$	Identification
S broad	6.28	{002} Phase 1 and Phase 2 superimposed
F	3.44	Li_xMoO_2 (see Fig. 16a)
F	3.14	{004} Phase 1 and Phase 2 superimposed
VF	2.86	{100} Phase 2
S	2.74	{100} Phase 1
M	2.68	{101} Phase 1
VF	≈ 2.60	{102} Phase 2
M	2.51	{102} Phase 1
F	2.43	Li_xMoO_2
S	2.28	{103} Phase 1
VF	≈ 2.11	{104} Phase 2

Remaining lines are those of 2H-MoS_2.

c) Phase 2 (c = 2 x 6.17 Å, a = 3.24 Å)

$I_{obs.}$	$d_{obs.}$	$d_{calc.}$	Identification
S	6.17	6.17	{002}
M	3.43		Li_xMoO_2 (see Fig. 16a)
VF	2.99		LiCl
M broad	2.78	2.81	{100}
M broad	2.56	2.55	{102}
M	2.43		Li_xMoO_2
VF	≃ 2.28	2.32	{103}
F V broad	≃ 2.07	2.08	{104}
F broad	1.71		Li_xMoO_2
F broad	1.62	1.62	{110}
F V broad	≃ 1.55	1.57	{112}

LiCl is an insoluble impurity found in the LiBr/PC electrolyte.

d) Phase 2 (c = 2 x 6.40 Å, a = 3.28 Å)

$I_{obs.}$	$d_{obs.}$	$d_{calc.}$	Identification
S	6.40	6.40	{002}
F	3.43		Li_xMoO_2 (see Fig. 16a)
VF	≃ 3.20	3.20	{004}
M	2.84	2.84	{100}
S V broad	≃ 2.60	2.60	{102}
F	2.44		Li_xMoO_2
M V broad	≃ 2.13	2.12	{104}
VF	≃ 1.89	1.90	{105}
F	1.72	1.71	Li_xMoO_2, {106}
F	1.64	1.64	{110}
F broad	1.59	1.59	{112}

e) Phase 2 (c = 2 x 6.33 Å, a = 3.34 Å)

$I_{obs.}$	$d_{obs.}$	$d_{calc.}$	Identification
S	6.33	6.33	{002}
VF	≃ 3.50		Li_xMoO_2 (see Fig. 16b)
VF	≃ 3.17	3.17	{004}
M broad	2.89	2.89	{100}
S V broad	≃ 2.64	2.64	{102}
F	≃ 2.43		Li_xMoO_2
M V broad	≃ 2.14	2.14	{104}
M broad	1.68	1.70, 1.67	{106}, {110}
VF	≃ 1.58	1.62	{112}

f) Phase 2 ($c = 2 \times 6.31$ Å, $a = 3.36$ Å)

$I_{obs.}$	$d_{obs.}$	$d_{calc.}$	Identification
S	6.31	6.31	{002}
VF	3.65		Li_xMoO_2 (see Fig. 16d)
M broad	2.92	2.91	{100}
S broad	2.64	2.64	{102}
F	2.44		Li_xMoO_2
M V broad	≃ 2.09	2.14	{104}
F broad	1.69	1.70, 1.68	{106},{110}

g) Phase 2 → 3 transition

$I_{obs.}$	$d_{obs.}$	Identification
F	6.30	{002} Phase 2 (Table 2e)
F	3.43	Li_xMoO_2 (see Fig. 16a)
VF	≃ 3.27	Li_2S ?
F	2.89	{100}
F	2.63	{102}
VF	2.42	Li_xMoO_2

h) Phase 3

$I_{obs.}$	$d_{obs.}$	Identification
F ring	6.3 → upper limit of film	{002}
F	3.44	Li_xMoO_2 (see Fig. 16a)

i) Phase 2 → 1 transition

Spectrum is that of 2H-MoS_2 except that the lines are broader than usual. This is suspected to be due to some non-uniform strain still present in the lattice. Li_xMoO_2 lines appear here at 3.43 Å, 2.43 Å, and 1.71 Å.

j) Phase 2 cathode washed in methanol.

Spectrum is that of 2H-MoS_2 with one extra line at ≃ 10.3 Å, possibly indicative of a superlattice. The lines in this pattern are all sharp, implying that the phase 2 line broadening is not due to small crystallite size.

MoO_2 cathodes were prepared by partially reducing MoO_3. Cells were then constructed in the same manner as the MoS_2 cells (Sect. 4.2). Patterns of Li_xMoO_2 compounds were obtained following the same experimental procedure as outlined in Sections 4.3 and 4.4. Mo metal is present as an impurity in most of the samples since some MoO_3 is completely reduced in the cathode preparation process. The spectra of four different Li_xMoO_2 compounds are shown in Fig. 16. The MoO_2 cells apparently also undergo a self-recharge, but possibly at a different rate than MoS_2 cells. As can be seen, the voltages corresponding to the Li_xMoO_2 spectra in Fig. 16 do not always match those corresponding to spectra in Fig. 15. This may be due to inhomogeneity in the sample during the self-recharging process.

The observed line spectra of those patterns in Fig. 16 are given in Table 3.

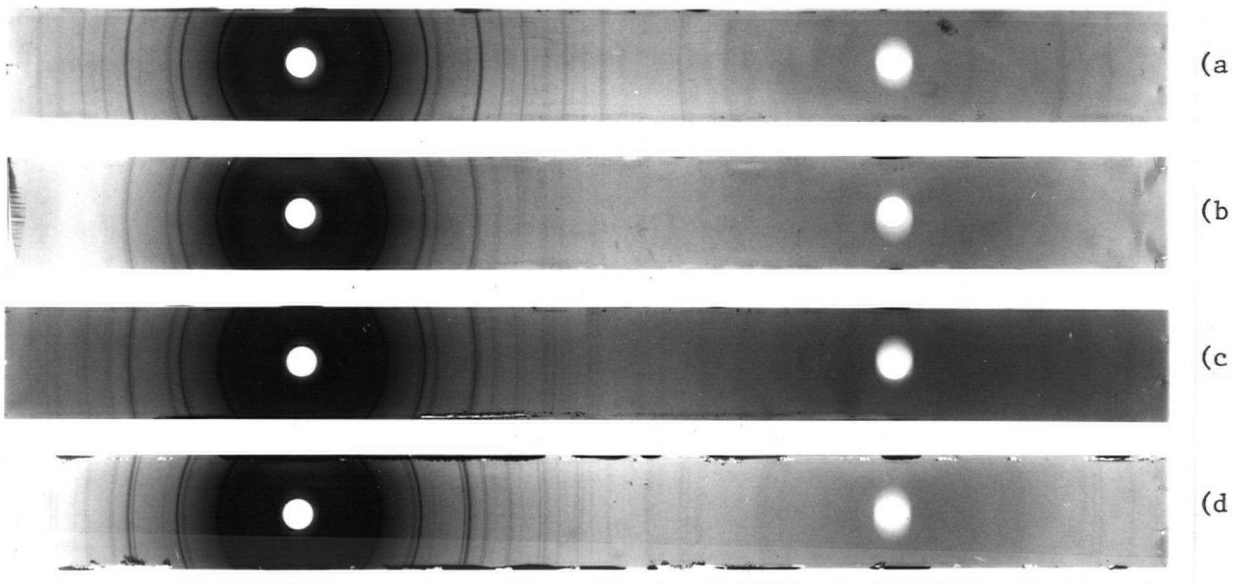

Fig. 16 - Li_xMoO_2 spectra

a) MoO_2 x = 0

b) Li_xMoO_2 (discharged to 1.6 V)

c) Li_xMoO_2 (discharged to 1.5 V)

d) Li_xMoO_2 (discharged to 1 V)

Table 3

Line spectra of Li_xMoO_2 patterns in Fig. 16

a)

$I_{obs.}$	$d_{obs.}$	
VS	3.43	
S	2.44	
M	2.42	
F	2.23	← Mo
VF	2.17	metal
F	1.84	
M } overlap	1.71	
M broad }		
F	1.53	
F	1.40	

+ others

b)

$I_{obs.}$	$d_{obs.}$	
F	3.57	
S	3.49	
S	2.45	
F	2.39	
F	2.22	← Mo
VF	1.78	metal
M	1.75	
F	1.71	

+ others

c)

$I_{obs.}$	$d_{obs.}$	
S	3.57	
M	3.46	
F	2.53	
S	2.44	
M broad	≃ 2.22	← Mo
F	1.79	metal
S	1.76	

+ others

d)

$I_{obs.}$	$d_{obs.}$	
VS	3.66	
M	2.61	
M	2.56	
S	2.45	
VF	2.30	
F	2.21	← Mo
S	1.83	metal
S broad	1.78	

+ others

Appendix B

Line broadening

Several X-ray patterns representative of intercalated MoS_2 appear in Fig. 15. The diffraction lines in most samples are much broader than in unintercalated MoS_2, and will thus appear fainter than narrow lines of the same integrated intensity. This line broadening, at least in phase 2, is apparently caused by the presence of non-uniform strain in the crystal lattice. Stresses arise in the lattice when the material undergoes its phase transitions (Sections 4.2 and 4.4).

Line broadening can also be due to small crystallite size or inhomogeneity of the sample. If the sample grains are less than $\approx 10^{-5}$ cm in size, then there are not enough lattice planes in a grain for complete destructive interference of off-angle diffracted beams. The result is line broadening, becoming worse as grain size decreases. An inhomogeneous sample, consisting of crystals of similar but not identical structures, will produce many similar but not identical X-ray spectra that can overlap with the net result being a pattern with broad lines. These effects have been ruled out as the major cause of line broadening in phase 2 from the reasoning to follow.

On a macroscopic scale, considerable cracking of layer compounds has been observed upon intercalation (Chianelli 1976). At first, it was thought that on a microscopic scale, similar cracking of the cathode material into small grains took place. However, the following experiment demonstrates that such an effect is not the cause of line broadening. After undergoing the phase $1 \rightarrow 2$ transition, samples exhibit line broadening. Washing such a sample in methanol removes much of the intercalated lithium, and the cathode material reverts from black to its original gray

colour. The subsequent X-ray pattern is as sharp as that of unintercalated MoS_2 (Fig. 15j).(The spectra is that of pure 2H-MoS_2 with one extra line at 10.3 Å, perhaps indicative of a superlattice.) If the lattice were stressed when lithium is intercalated, the removal of the lithium could remove the stress. But, if the sample split into very small grains, broad X-ray lines would be expected from any resulting product too. So far, it has not been possible to demonstrate that line broadening in phase 3 is not due to small crystallite size.

Inhomogeneous distribution of the intercalated lithium is also unlikely to be the main cause of line broadening. Samples from all phases have been X-rayed after being allowed to equilibrate for several days with no apparent reduction in line breadth. (Cells are capable of high discharge rates in phases 2 and 3. Over several days, the intercalated lithium is expected to have more than adequate time to diffuse evenly in the sandwich gaps.)

Appendix C

Errors in Phase 2 measurements

Line broadening

It is difficult to determine the exact positions of the lines in phase 2 spectra, because they are so broad. Generally, the broadening gets worse with increasing Bragg angle. The layer spacing, given in Figs. 12 and 13, was mainly determined from the {002} reflection (assuming a 2 layer unit cell). Other lines in the pattern are not very sensitive to small changes in the layer spacing and to make matters worse, these lines were quite broad. Similarly, the a axis was determined from the {100} reflection and/or the {110} reflection, depending on the quality of these lines. (The {110} line is more sensitive to changes in a, but sometimes its position could not be accurately determined. For example, the {106} line is expected to overlap it if the cell were discharged to the C - E region in Fig. 4.) Several measurements of each line were made. The maximum uncertainties expected in the layer spacing and the a axis are $\simeq \pm 0.03$ Å and $\simeq \pm 0.02$ Å respectively. The other broader lines in the pattern roughly confirm the values determined by these measurements. Other errors in the lattice parameter values are negligible compared to those introduced by line broadening.

Self-recharge

The self-recharging characteristic of the cells introduces an uncertainty in the discharge state as represented by the cell voltage. The limit of the cell voltage drift was determined from the dummy cathode. This assumes that the material scraped off the cathode (in a minimum volume of electrolyte) does not self-recharge faster than the dummy (suspended above the electrolyte in the cell, but still wet with a

significant amount of electrolyte). In fact, subsequent X-ray patterns from samples run weeks earlier suggested that the self-recharge (as represented by actual structural change) may be slowed down in the capillary configuration. The actual discharge state of the X-ray specimen, then, may be quite different from that of the dummy. For this reason, the specimen discharge state, as given by the cell voltage, was taken to be the initial discharge state with an error bar to indicate the amount of drift of the dummy cathode. The self-recharge phenomena causes the greatest uncertainties in the phase 2 data.

Appendix D

Intensity calculations

Attempts were made to fit the X-ray spectrum of a phase 2 cathode discharged to point C on the discharge curve in Fig. 4. The calculated patterns for the three most common structures are presented here in Table 4. These are 2H-MoS_2, 2H-NbS_2, and 1T-TiS_2 type structures. The calculated intensities depend mainly on the positions of the Mo atoms (being the strongest scatterers of the X-rays). Thus the calculated spectra of 2H-NbS_2 and 1T-TiS_2 type structures are quite similar, since the Mo atom positions in both are identical. Also presented in this appendix is an example of the agreement to be expected between the observed and the calculated line intensities (Table 5).

In all these calculations, the lithium atoms were ignored as they are very weak scatterers. The sandwich height was assumed to be the 2H-MoS_2 value of 3.19 Å. (The gross features of the calculated spectrum are not changed significantly even if the sandwich height is varied by ± 0.15 Å. In fact, the layer spacing in phase 2 has only increased ≃ 0.2 Å from the 2H-MoS_2 value.) The line intensities were then calculated according to the procedure outlined in Sect. 2.2. The fractional coordinates for the atomic positions in the unit cell are -

2H-MoS_2 type structure :

S - (0,0,0)
- (0,0,3.19/c)
- (2/3,1/3,1/2)
- (2/3,1/3,1/2 + 3.19/c)

Mo - (2/3,1/3,3.19/2c)
- (0,0,1/2 + 3.19/2c)

$2H\text{-}NbS_2$ type structure :

S - (0,0,0,)
- (0,0,3.19/c)
- (1/3,2/3,1/2)
- (1/3,2/3,1/2 + 3.19/c)

Mo - (2/3,1/3,3.19/2c)
- (2/3,1/3,1/2 + 3.19/2c)

$1T\text{-}TiS_2$ type structure :

S - (0,0,0)
- (1/3,2/3,3.19/c)

Mo - (2/3,1/3,3.19/2c)

Table 4

Calculated intensities for various phase 2 structure candidates

(At point C on the discharge curve in Fig. 4)

$d_{obs.}$(A)	$I_{obs.}$	Calculated intensities: 2H-MoS_2 type	2H-NbS_2 type	1T-TiS_2 type	$d_{calc.}$(A)	Indices for 2H- type, 1T- type	
		0	0		12.7	{001}	
6.33	S	100	100	100	6.33	{002}	{001}
		0	0		4.22	{003}	
3.17	VF	2	2	2	3.16	{004}	{002}
2.89	M	31	20	20	2.89	{100}	{100}
		18	14		2.82	{101}	
2.64	S	17	71	91	2.63	{102}	{101}, {$\bar{1}$01}
		0	0		2.53	{005}	
		84	9		2.39	{103}	
2.14	M	1	66	65	2.14	{104}	{102}, {$\bar{1}$02}
		6	6	6	2.11	{006}	{003}
		40	4		1.90	{105}	
		0	0		1.81	{007}	
1.68	M	5	17	23	1.70	{106}	{103}, {$\bar{1}$03}
		22	22	22	1.67	{110}	{110}
		0	0		1.66	{111}	
1.62	VF	14	14	14	1.62	{112}	{111}
		6	6	6	1.58	{008}	{004}
		0	0		1.55	{113}	
		2	2		1.53	{107}	
		1	1	1	1.48	{114}	{112}
		3	2	2	1.45	{200}	{200}
		2	2		1.44	{201}	
		2	9	12	1.41	{202}	{201}, {$\bar{2}$01}
		0	0		1.41	{009}	
		0	0		1.39	{115}	
		6	4	4	1.39	{108}	{104}, {$\bar{1}$04}
		13	1		1.37	{203}	
		0	13	12	1.32	{204}	{202}, {$\bar{2}$02}
		7	8	7	1.31	{116}	{113}
		1	1	1	1.27	{0010}	{005}
		1	1		1.26	{109}	
		10	1		1.26	{205}	
		0	0		1.23	{117}	
		1	5	6	1.19	{206}	{203}, {$\bar{2}$03}

S = Strong
M = Moderate
VF = Very Faint

a = 3.34 A
c = 2 x 6.33 A
sandwich height = 3.19 A

Table 5

Comparison between observed and calculated line intensities in 2H-MoS_2.

$I^*_{obs.}$	$I_{calc.}$	$d_{calc.}$	hkl
	0	12.3	{001}
100	100	6.15	{002}
	0	4.10	{003}
4	2	3.08	{004}
16	31	2.74	{100}
9	18	2.67	{101}
8	16	2.50	{102}
	0	2.46	{005}
45	87	2.28	{103}
14	8	2.05	{006}
	1	2.04	{104}
25	37	1.83	{105}
	0	1.76	{007}
4	5	1.64	{106}
11	21	1.58	{110}
	0	1.57	{111}
12	6	1.54	{008}
	13	1.53	{112}
2	2	1.48	{107}
	0	1.47	{113}
	1	1.41	{114}
2	3	1.37	{200}
	0	1.37	{009}
	2	1.36	{201}
4	6	1.34	{108}
	2	1.34	{202}
	0	1.33	{115}
5	13	1.30	{203}
4	9	1.25	{116}
	0	1.25	{204}
2	1	1.23	{0010}
1	2	1.22	{109}
4	9	1.20	{205}
	0	1.17	{117}
	2	1.14	{206}

etc.

a = 3.16 Å, c = 2 x 6.15 Å, sandwich height = 3.19 Å

* National Bureau of Standards data (Powder Diffraction File - McClune 1977)